Flexural-torsional buckling of austenitic stainless steel I-section beam-columns: Testing, numerical modelling and design

Merih Kucukler[a,*], Leroy Gardner[b], Yidu Bu[b]

[a]*School of Engineering, University of Warwick, Coventry, CV4 7AL, UK*
[b]*Department of Civil and Environmental Engineering, Imperial College London, London, SW7 2AZ, UK*

Abstract

The flexural-torsional buckling response and design of stainless steel I-section beam-columns are investigated in this paper. First, a series of laboratory tests on laser-welded stainless steel I-section beam-columns susceptible to flexural-torsional buckling is presented. The results obtained are supplemented by further data generated by means of numerical parametric studies on both conventionally arc-welded and laser-welded stainless steel members covering a wide range of member slenderness and combinations of loading. Existing provisions for the design of welded stainless steel I-section elements against flexural-torsional buckling are then assessed and found to require improvement. Finally, new formulae for the design of stainless steel I-section beam-columns susceptible to flexural-torsional buckling are proposed. The new proposals yield improved accuracy and consistency over existing provisions and their suitability for inclusion in the upcoming version of the European structural stainless steel design code EN 1993-1-4 is confirmed by reliability analysis in accordance with EN 1990.

Keywords: Beam-column tests, Buckling, Experiments, Flexural-torsional buckling, Numerical modelling, Stainless steel, Testing

1. Introduction

Stainless steel is being increasingly utilised in the construction industry owing to its excellent durability even in the harshest environmental conditions, sound mechanical properties and aesthetic appearance [1]. Thus far, cold-formed stainless steel elements have been the primary product types used in construction, and have benefited from the most extensive research and the widest coverage in structural stainless steel design standards [2–4]. However, the demands to achieve higher structural resistances for stainless steel members have brought about the need for the use of larger sections fabricated through the welding of individual hot-rolled stainless steel plates. New manufacturing techniques for such members,

*Corresponding author
Email addresses: merih.kucukler@warwick.ac.uk (Merih Kucukler), leroy.gardner@imperial.ac.uk (Leroy Gardner), yidubu@mail.tsinghua.edu.cn (Yidu Bu)

such as high-precision laser-welding have also recently emerged. These developments have created the need for developing a better understanding of the structural response of both conventionally arc-welded and laser-welded stainless steel members, and this is the aim of the present paper.

To investigate the structural behaviour of welded I-section stainless steel elements, a research programme involving physical laboratory experiments, advanced numerical modelling and development of design guidance was initiated by Gardner et al. [5], involving residual stress measurements, tensile coupon, stub column and column flexural buckling tests [5], bending tests on laterally restrained beams [6] and tests on laterally-restrained beam-columns [7]. This research resulted in the development of a new residual stress pattern [5], column buckling curves [8] and beam-column design rules [7] for laser-welded stainless steel elements. For the case of conventionally arc-welded stainless steel I-section beam-columns, a series of physical experiments has been carried out by Yang et al. [9], which was complemented by numerical studies and the development of design guidance. Zheng et al. [10] and Burgan et al. [11] also reported a series of experiments on stainless steel welded I-section members. However, to date, there have been no studies into the flexural-torsional buckling response of welded stainless steel elements and there is thus currently an absence of verified structural design guidance for this mode of failure.

Extending the work carried out on the behaviour of laser-welded stainless steel I-section elements [5–8], a research study comprising (i) physical laboratory testing, (ii) advanced non-linear finite element modelling and (iii) the development of design guidance for austenitic stainless steel welded I-section beam-columns susceptible to flexural-torsional buckling is presented in this paper. First, physical laboratory tests are reported on five laser-welded stainless steel I-section beam-columns. Following the physical experimental programme, shell finite element models able to replicate the response of welded I-section stainless steel elements are created and validated against the experiments conducted in this study. Using the validated finite element models, a wide range of parametric studies are performed considering various cross-section proportions, loading conditions and member slenderness. The behaviour of both conventionally arc-welded and laser-welded stainless steel beam-columns is considered. The accuracy of existing design methods for stainless steel I-section beam-columns susceptible to flexural-torsional buckling – those set out in the European structural stainless steel code EN 1993-1-4 [2] and the North American AISC Design Guide 27 [12] – as well as those proposed by Greiner and Kettler [13] is investigated and shortcomings are highlighted. Utilising the results from the physical laboratory tests and the comprehensive parametric studies, a new design method for conventionally arc-welded and laser-welded stainless steel beam-columns is proposed, whose accuracy, reliability and safety are thoroughly verified.

2. Experimental investigation

2.1. Introduction

To investigate the structural response of laser-welded stainless steel I-section beam-columns susceptible to flexural-torsional buckling, a physical experimental programme was

performed in the Structures Laboratory of Imperial College London. The testing programme comprised five grade 1.4301 austenitic stainless steel laser-welded beam-column specimens with an I-50×50×4×4 cross-section; the measurements of the geometrical and material properties, initial geometric imperfections and residual stresses are presented. Falling into the Class 1 category according to EN 1993-1-4 [2], the considered I-50×50×4×4 cross-section, which adopts the following designation system: I - section height (h) × flange width (b_f) × web thickness (t_w) × flange thickness (t_f), was fabricated through the laser-welding of individual hot-rolled grade 1.4301 austenitic stainless steel plates. A detailed description of the experimental setup and procedure, and the key findings of the experimental programme are presented in this section.

2.2. Material properties

Both tensile and compressive material properties of the specimens were measured. As reported in [5], the tensile material properties were obtained through tensile coupon tests carried out in line with the provisions of EN ISO 6892 [14], whereas the compressive material properties were determined by means of stub column tests, as detailed in [6]. The tensile and compressive material properties of the specimens are set out in Table 1, where E is the Young's modulus, f_y and $f_{1.0}$ are the 0.2% and 1% proof strengths respectively, f_u is the ultimate tensile strength, ϵ_u is the strain at the ultimate tensile strength, and ϵ_f is the fracture strain measured over the standard gauge length [14]. Gardner et al. [5] and Bu and Gardner [6] fitted two-stage compound Ramberg-Osgood material models [15–17] to the measured tensile and compressive stress-strain curves respectively; the fitted strain hardening exponents n, $m_{1.0}$ and m_u [1] for both tension and compression are displayed in Table 1. It should be noted that in the case of the compressive material properties, local buckling of the stub columns prevented the attainment of f_u, ϵ_u and ϵ_f. Thus, the Ramberg-Osgood exponents n and $m_{1.0}$ were fitted to the available stress-strain data up to the point where local buckling occurred; beyond this point the stress-strain curve was extrapolated in parallel with the corresponding tensile stress-strain curve up to the ultimate tensile stress [6].

2.3. Residual stresses

In accordance with the procedure recommended by the Structural Stability Research Council [18], the residual stresses existing in the laser-welded sections were measured by means of the sectioning method [19] as described in detail in [5]. On the basis of the measurements made in [5], as well as those made on laser-welded stainless steel T-sections reported in [20], a generic residual stress pattern for laser-welded stainless steel I-sections was put forward in [5]. The recommended residual stress pattern [5] is of the same general form as that proposed for arc-welded stainless steel I-sections in [21]. This generic pattern is illustrated in Fig. 1; the values of the parameters used in the generic residual stress pattern for laser-welded I-sections [5] and conventionally arc-welded I-sections [21] are provided in Table 2. As can be seen from the table, the laser-welded sections have lower residual stresses than those fabricated through conventional arc-welding owing to the lower heat input and higher-precision of the fabrication procedure. The residual stress pattern displayed in Fig.

1 is used in conjunction with the corresponding parameters for laser-welded and arc-welded stainless steel sections given in Table 2 in the finite element modelling presented in Section 3.

2.4. Flexural-torsional buckling tests on laser-welded I-section beam-columns

To examine the flexural-torsional buckling response and load carrying capacities of stainless steel structural elements, five laterally-unrestrained laser-welded grade 1.4301 austenitic stainless steel I-section beam-columns subjected to axial compression plus major axis bending were tested in this study. One cross-section size, I-50×50×4×4, was considered in the experimental programme and all the specimens had a nominal length of 1014 mm. Note that since stainless steel I-sections are not typically available as hot-rolled products, welded cross-sections are generally employed in their place. The tested profile is at the lighter end of available section sizes and, although size effects have not been explicitly examined herein, the proportions of this section are also representative of larger section sizes; a wider range of proportions are considered in the numerical parametric study presented in Section 3.5. The axial loads were eccentrically applied to the specimens with eccentricity values ranging between 5 mm and 150 mm, thereby enabling the simultaneous application of the axial compression and major axis bending moments to the specimens with different bending moment-to-axial compressive load ratios.

Prior to the testing of the specimens, their geometric properties were measured, which are set out in Table 3, where h and b_f are the overall depth and width of the cross-section, t_w and t_f are the web and flange thickness respectively and L is the length of the specimen. Note that the specimen IDs were specified such that their numbers correspond to those of the specimens tested by [7] with the same eccentricity values. In accordance with the procedure adopted by [22], the global geometric imperfections of the specimens were measured prior to the member tests by (i) placing each specimen on a milling machine and (ii) using a Linear Variable Displacement Transducer (LVDT) attached to the head of the milling machine to measure the deviations along the longitudinal axis of the specimen, which was secured to the moving machine bed. The global geometrical imperfections of the specimens about the major axis, measured at their mid-heights, ω_g are provided in Table 3. Measurements of initial local imperfections ω_l were not made for each test specimen, but the maximum local imperfection magnitude, as obtained from measurements made on stub columns of the same section size and cut from the same delivered batch, was 0.23 mm (i.e. $\omega_l = 0.23$ mm)[5].

The experiments were carried out by means of an Instron Servo-hydraulic Testing Machine with a capacity of 2000 kN. Displacement control was used to drive the testing machine at a constant rate of 0.4 mm/min. As illustrated in Fig. 2, knife edges and wedge plates were utilised to establish pin-ended support conditions about the major axis at the top and bottom ends. A pair of clamp plates were used at the ends to suppress the rotations about the minor axis and twists, leading to pin-ended support conditions about the major axis and fixed-ended support conditions about the minor axis for the specimens. End-plates with a thickness of 12 mm were also welded to the specimens, which prevented any possible warping deformations at the ends. The height of each pair of knife edges and wedge plates was 75 mm.

Based on the end-support conditions, the height of the each pair of knife edges and wedge plates and the measured geometrical properties of the specimens, the in-plane (i.e. in the plane of bending) and out-of-plane buckling lengths (i.e. $L_{cr,y}$ and $L_{cr,z}$) and the non-dimensional slenderness of the specimens for the flexural buckling about the major $\overline{\lambda}_y$ and minor $\overline{\lambda}_z$ axes and for lateral-torsional buckling $\overline{\lambda}_{LT}$ are provided in Table 4. Due to the presence of the clamp plates restraining the end-rotations about the minor axis, the minor axis buckling lengths $L_{cr,z}$ are equal to the half of the actual member lengths (i.e. $L_{cr,z} = L/2$), while the major axis buckling lengths are equal to the member lengths plus the total length of the wedge plates and knife edges at both ends (i.e. $L_{cr,y} = L + 150$ mm). Note that the non-dimensional slendernesses (i.e. $\overline{\lambda}_y$, $\overline{\lambda}_z$ and $\overline{\lambda}_{LT}$) given in Table 4 were determined using the compressive material properties of the specimens provided in Table 1. The non-dimensional slenderness for the major axis and minor axis flexural buckling were calculated by taking the square root of the ratios between the axial cross-section resistances Af_y and the corresponding elastic flexural buckling loads $N_{cr,y}$ and $N_{cr,z}$ (i.e. $\overline{\lambda}_y = \sqrt{Af_y/N_{cr,y}}$ and $\overline{\lambda}_z = \sqrt{Af_y/N_{cr,z}}$), whereas the non-dimensional LTB slenderness was determined by taking the square root of the ratios between major axis plastic bending moment resistances $W_{pl,y}f_y$ and the elastic critical buckling moments M_{cr} (i.e. $\overline{\lambda}_{LT} = W_{pl,y}f_y/M_{cr}$).

In the experiments, the desired initial load eccentricities were achieved by positioning the specimens in the test rig such that the distances between the centrelines of the specimens and the knife edges were equal to the target eccentricity values. The same initial loading eccentricities were applied at both ends of the members, thus inducing a constant first-order major axis bending moment in addition to axial compression.

To record the mid-height out-of-plane deflections and twists as a result of flexural-torsional buckling in addition to the mid-height in-plane deformations, a series of string potentiometers were employed. The configuration of the string potentiometers is shown in Fig. 3. The combined measurements from the string potentiometers were used to determine the mid-height deflections and twists of the specimens through simple geometrical relationships. To measure the end rotations, two inclinometers were placed at the ends of the specimens, while the end-shortening was recorded by means of a linear variable differential transducer (LVDT) within the testing machine. As shown in Fig. 3, two strain gauges were affixed to the middle of the flanges at the mid-height of the specimens, thereby recording the maximum compressive and maximum tensile (or the minimum compressive, depending on the magnitude of the eccentricity) longitudinal strains resulting from the major axis bending moment and axial compression. Following the procedure described in [7], the strain gauges were also utilised to measure the initial loading eccentricities using the following expression:

$$e_m = \frac{EI_y\left(\epsilon_{max} - \epsilon_{min}\right)}{N_{Ed}h} - \left(\omega_g + u\right) \tag{1}$$

where I_y is the second moment of area about the major axis, ϵ_{max} and ϵ_{min} are the maximum and minimum compressive strains recorded by the strain gauges, N_{Ed} is the applied axial load, ω_g is the measured global imperfection of the specimen at mid-height and u is the in-plane mid-height deformation of the specimen. The measured values of the initial eccentricities e_m are compared against the nominal target values e_n in Table 3, showing that the

measured eccentricities e_m are very close to the nominal target values e_n. During testing, all data were recorded at one-second intervals by means of the DATASCAN data acquisition system.

A summary of the experimental findings is presented in Table 5, where $N_{ult,test}$ and $M_{y,ult,test}$ are the ultimate axial compression and first-order major axis bending moment at the member ends, respectively, obtained from the experiments and $u_{ult,test}$ is the in-plane deflection at the ultimate loads. Note that the ultimate first-order bending moment values $M_{y,ult,test}$ were determined by multiplying the ultimate axial compression values $N_{ult,test}$ by the measured initial eccentricities e_m, i.e. $M_{y,ult,test} = N_{ult,test}e_m$. As can be seen from Table 5, the greater the level of the eccentricity, the lower the axial ultimate load carrying capacity $N_{ult,test}$ of the specimen. The failure modes of the specimens are displayed in Fig. 4. The applied axial load N_{Ed} versus mid-height deformation paths of the specimens are provided in Fig. 5 with respect to the in-plane deflection u, out-of-plane deflection v and twist θ at mid-height. The presented tests results are utilised in Section 3 for the validation of the numerical models and in Sections 4 and 5 for the assessment of existing and new design provisions, respectively.

3. Numerical modelling

3.1. Introduction

In this section, finite element models are created and validated against the experimental results obtained in the previous section. The validated finite element models are employed in the following sections to carry out extensive parametric studies into the flexural-torsional buckling response of laser-welded and conventionally arc-welded austenitic stainless steel beam columns, providing comprehensive structural performance data that is used to develop a new design method for the flexural-torsional buckling assessment of welded stainless steel members in Section 5.

3.2. Modelling assumptions

The finite element models were created using the finite element analysis software Abaqus [23]. Denoted as S4R in the Abaqus element library [23], the four-noded general purpose, reduced integration shell element, which allows for transverse shear deformations and finite membrane strains, was used to create all the finite element models. The finite element models were meshed by taking the element size equal to the cross-section thickness. To avoid overlapping of the flange and web plates, the flange plates were offset by half the flange thickness in accordance with the approach adopted by [24–26]. The default Simpson integration method with five integration points through the thickness of the elements was used. The Poisson's ratio was taken as 0.3 in the elastic range and 0.5 in the plastic range by defining the effective Poisson's ratio as 0.5, thereby allowing for the change of cross-sectional area under loading. The two-stage compound Ramberg-Osgood material model put forward by Gardner and Ashraf [16] was utilised to define the material stress-strain curves, using the experimentally measured engineering stress-strain properties and the corresponding fitted Ramberg-Osgood parameters (i.e. n and $n_{0.2-1.0}$) provided in Table 1. Since the constitutive

formulations of Abaqus [23] adopt the Cauchy (true) stress-strain assumption for the adopted element type, the measured engineering stress-strain response ($\sigma_{nom} - \epsilon^{pl}_{nom}$) was transformed into the true stress-log plastic strain ($\sigma_{true} - \epsilon^{pl}_{true}$) and input into Abaqus [23], where the true stress values were determined as $\sigma_{true} = \sigma_{nom}(1 + \epsilon_{nom})$, while the log plastic strain values were calculated as $\epsilon^{pl}_{ln} = ln(1+\epsilon_{nom}) - \sigma_{true}/E$. It should be noted that for the case of compression, the true stress-log plastic strain values (i.e. $\sigma_{true,comp} - \epsilon^{pl}_{ln,comp}$) were determined using the negative values of the engineering stresses σ_{nom} and strains ϵ_{nom}, and the absolute values of $\sigma_{true,comp} - \epsilon_{ln,comp}$ were input into Abaqus [23]. In the validation of the finite element models, the measured compressive and tensile material properties were assigned to the elements subjected to the compressive and tensile stresses respectively, which were determined on the basis of the applied first-order bending moment and axial compression values at the member ends. Note that this approximate allowance for anisotropy does not take into account changes to the direction of loading (i.e. compression to tension and vice versa) arising due to the development of second-order bending moments, though the effect of this shortcoming is small because the degree of anisotropy is relatively mild.

The boundary conditions of the finite element models were defined in accordance with those adopted in the experiments during the validation study. The degrees-of-freedom of all the nodes constituting each end section were constrained to an eccentric reference point by means of coupling constraints. The coordinates of the reference point were defined considering the corresponding desired eccentricity values e_m; in the validation of the finite element models, the e_m values provided in Table 3 were used. To represent the distance between the end of the specimen and the tip of the knife-edge, the reference points were offset longitudinally from each end by 75 mm. The boundary conditions were defined at the reference points such that the pin-ended in-plane and fix-ended out-of-plane support conditions were simulated in accordance with the experiments. The axial compression was applied at the eccentric reference points, thereby subjecting the finite element models to axial compression plus uniform first-order major axis bending.

3.3. Geometric imperfections and residual stresses

Utilising the lowest global and local buckling modes obtained from priorly performed Linear Eigenvalue Analyses (LEA) to define the imperfection shapes, both global and local geometric imperfections were included in the Geometrically and Materially Nonlinear Analyses with Imperfections (GMNIA) of the finite element models. In the validation of the finite element models, the corresponding measured in-plane global geometric imperfections ω_g at the mid-height of the members given in Table 3 were used to scale the lowest global buckling modes if they were in the in-plane direction, while the lowest global buckling modes were scaled to 1/1000 of the member length L if they were in the out-of-plane direction. In the parametric studies, the lowest global buckling modes were scaled to 1/1000 of the member length L (i.e. $\omega_g = L/1000$), in line with [27–29]. The local imperfections were assigned to the finite element models using their corresponding lowest local buckling mode shapes. While the local buckling modes were scaled to the experimentally measured maximum value of $\omega_l = 0.23$ mm for the considered I-50×50×4×4 section in the validation study based on the measurements presented in [5], they were scaled to 80% of the fabrication tolerances for

welded steel members provided in EN 1090-2 [30] in accordance with the provisions of EN 1993-1-5 [31] in the parametric studies. Thus, the lowest local buckling modes were scaled to 80% of 1/100 of the web heights h_w (i.e. $\omega_l = 0.8h_w/100$) if the maximum normalised deflections observed in the LEA were within the webs, while the lowest local buckling modes were scaled to 80% of 1/100 of the flange widths b_f if the maximum normalised displacements observed in the LEA were within the flanges (i.e. $\omega_l = 0.8b_f/100$). Examples of the global and local buckling modes used to define the geometric imperfections in the finite element models are illustrated in Fig. 7. As can be seen from the figure, the global geometric imperfection involves both initial out-of-straightness about the minor axis and twist.

Residual stresses were incorporated into the finite element models using the generic residual stress pattern for welded I-sections shown in Fig. 1; the residual stresses were applied to the finite element models within a separate step finalised with the achievement of the equilibrium prior to the application of the loading. Both conventionally arc-welded and laser-welded stainless steel members were considered by adopting the corresponding model parameters given in Table 2. Owing to the nonlinear material stress-strain response of stainless steel, the application of residual stresses results in permanent strains; hence the residual plastic strains $\epsilon_{res,pl}$ corresponding to the assigned residual stresses σ_{res} were also applied to the finite element models. Considering the two-stage compound Ramberg-Osgood stress-strain relationship [16] adopted in this paper, the following expression was used to define the residual plastic strains $\epsilon_{res,pl}$ at the cross-section integration points in the finite element models [32]:

$$\epsilon_{res,pl} = 0.002 \left(\frac{\sigma_{res}}{f_y} \right)^n , \tag{2}$$

where σ_{res} is the corresponding residual stress applied at the cross-section integration point. The application of the residual plastic strains $\epsilon_{res,pl}$ is necessary to ensure that the desired residual stress pattern shown in Fig. 1 is achieved after the equilibrium load step.

3.4. Validation of numerical models

Comparisons of the ultimate loads from the finite element models $N_{ult,FE}$ with those obtained from the physical laboratory tests $N_{ult,test}$ presented in the previous section are shown in Table 6, where the in-plane deflections at the ultimate loads determined through the finite element models $u_{ult,FE}$ are also compared against those observed in the experiments $u_{ult,test}$. As can be seen from the table, the ultimate loads obtained from the finite element models and the experiments are in close agreement in addition to a good correlation between the numerically and experimentally determined in-plane deflections at the ultimate loads, indicating that the finite element models are capable of accurately estimating the ultimate load carrying capacities of the stainless steel members. Additionally, the load versus mid-height in-plane deflection, load versus mid-height out-of-plane deflection and load versus mid-height twist paths obtained from the experiments and those determined through the finite element models are shown in Fig. 5. It can be seen from the figures that the correlation between the experimentally and numerically obtained load versus displacement paths

is very good, confirming the ability of the finite element models to replicate the physical response of stainless steel beam-columns experiencing flexural-torsional buckling. The load versus mid-height strain paths obtained from the experiments and finite element models are shown in Fig. 6 and can be seen to be also in good agreement. Discrepancies between the experimental and numerical paths in Figs. 5 and 6, particularly for specimen 50 LTB-2, are attributed to differences in local and global imperfections between the test specimens and numerical simulations. While global imperfection magnitudes were measured for each test specimen, only representative local imperfection magnitudes were obtained from measurements on stub columns cut from the same delivered lengths of material. Furthermore, detailed measurements of imperfection shapes were not made, but were assumed to follow the form of the elastic buckling modes in the numerical analyses. The failure modes observed in the experiments and the numerical models are compared in Fig. 8, where they can be seen to be very similar. The models are therefore considered to be validated and suitable for performing parametric studies, as presented in the following sub-section.

3.5. Parametric studies

Using the validated finite element models, extensive parametric studies considering a wide range of cross-section shapes, cross-section slenderness, bending moment-to-axial compressive load ratios and member slenderness were carried out to generate comprehensive structural performance data for conventionally arc-welded and laser-welded austenitic stainless steel beam-columns. The standardised material properties for austenitic stainless steel recommended in [33] and based on large number of data collected from the literature were utilised in the parametric studies.

In the parametric studies, a constant cross-section depth equal to that of the test specimens (i.e. $h = 50$ mm) was adopted, while four different flange widths were considered, leading to four cross-section aspect ratios h/b_f equal to 1.0, 1.5, 2.0 and 3.0 (i.e. $h/b_f = 1.0, 1.5, 2.0$ and 3.0). For each cross-section aspect ratio, three different values of flange thickness t_f and web thickness t_w were selected to generate a range of local slenderness covering cross-sections from Class 1 to Class 3 according to the slenderness limits set out in EN 1993-1-4 [2]. The flange and web thicknesses were selected such that the flange plate slenderness $\overline{\lambda}_{p,f}$ and the web plate slenderness $\overline{\lambda}_{p,f}$ of the modelled cross-sections were essentially the same; the flange and web plate slenderness were determined from eqs. (3) and (4) respectively, as given in EN 1993-1-5 [31]:

$$\overline{\lambda}_{p,f} = \sqrt{f_y / f_{cr,f}}, \tag{3}$$

$$\overline{\lambda}_{p,w} = \sqrt{f_y / f_{cr,w}}, \tag{4}$$

in which, $f_{cr,f}$ and $f_{cr,w}$ are the elastic buckling stresses of the flange and web plates, respectively. Beam-columns with seven different lengths L were modelled for each considered cross-section; the lengths of the columns for the each cross-section were selected such that their non-dimensional flexural buckling slendernesses about the minor axis $\overline{\lambda}_z$ ranged between 0.4 and 2.0 in increments of 0.4. Two additional lengths for each cross-section

corresponding to $\overline{\lambda}_z = 0.2$ and $\overline{\lambda}_z = 1.0$ were also taken into account. Five initial loading eccentricities, as adopted in the experimental study, ranging between 5 mm and 150 mm (i.e. $e_n = 5, 20, 40, 80$ and 150 mm), were applied to each considered beam-columns, thereby inducing a range of major-axis bending-to-axial compressive load ratios. The generic residual stress pattern shown in Fig. 1 in conjunction with the corresponding parameters for arc-welded and laser-welded sections were applied to the finite element models. In accordance with the numerical parametric studies carried out during the development of the EN 1993-1-1 beam-column design rules [29], fork-end support conditions were also adopted in the numerical parametric study models developed herein, as described in detail in [24]. All the considered members were subjected to axial compression plus constant major axis bending. In Section 4, the results of the parametric studies are utilised to assess the accuracy of existing design methods for the flexural-torsional buckling of welded stainless steel beam-columns, while in Section 5, the parametric results are used in the development and verification of new design provisions.

4. Assessment of existing design rules for stainless steel I-section beam-columns susceptible to flexural-torsional buckling

4.1. Introduction

In this section, three existing methods for the flexural-torsional buckling design of stainless steel beam-columns provided in (i) the European structural stainless steel design code EN 1993-1-4 [2], (ii) AISC Design Guide 27 [12] and (iii) the proposals of Greiner and Kettler [13] are assessed using both the experimental and numerical results obtained in this paper. In the accuracy assessment of the existing design methods for arc-welded stainless steel members, the experimental results provided by [9, 11, 34, 35] for laterally unrestrained beam-columns, beams and columns are used, while the results obtained from the experiments presented in this paper and those reported in [5] for columns buckling about the minor axis are utilised to assess the existing design methods for laser-welded beam-columns. As illustrated in Fig. 9, to assess the accuracy of each design method, the parameter ϵ corresponding to the ratios of the ultimate axial load carrying capacities obtained from the experiments and numerical models N_u to those obtained from the design method $N_{u,pred}$ is utilised, i.e. $\epsilon = N_u/N_{u,pred}$, where the beam-columns are assumed to be under proportional loading. Note that in Fig. 9, $N_{b,Rd}$ and $M_{b,Rd}$ are the column buckling and lateral-torsional buckling strengths determined using each design method and represent the end points of the design interaction curve, N_{Ed} and $M_{y,Ed}$ are the proportionally increasing applied axial loading and bending moment, and θ is the radial angle describing the relationship between the applied axial loading and bending moment, which is determined using the following expression:

$$\theta = tan^{-1}\left(\frac{N_{Ed}/N_{b,Rd}}{M_{y,Ed}/M_{b,Rd}}\right). \tag{5}$$

Fig. 9 shows that depending on the dominance of the applied axial loading and bending, the radial angle θ varies between 0° and 90° where $\theta = 0°$ and $\theta = 90°$ correspond to pure

bending and pure axial loading, respectively. A value of $\epsilon = N_u/N_{u,pred}$ greater than 1.0 indicates the safe-sided strength prediction.

Using the ϵ parameter, the accuracy of EN 1993-1-4 [2], AISC Design Guide 27 [12] and the proposals of Greiner and Kettler [13] are assessed against numerical results for conventionally arc-welded and laser-welded stainless steel beam-columns in Table 7, as well as against the experimental results of the five laser-welded stainless steel beam-columns obtained in this paper and the experimental results obtained for laterally unrestrained arc-welded beam-columns, beams and columns by Burgan et al. [11] and Yang et al. [9]. Note that in Table 7, ϵ_{av}, ϵ_{cov}, ϵ_{max} and ϵ_{min} are the average, coefficient of variation, maximum and minimum values of ϵ obtained for each design method. In the following sections, these three design methods will be briefly described and their accuracy with respect to the design of stainless steel beam-columns is discussed.

4.2. European structural stainless steel design code EN 1993-1-4 [2]

The European structural stainless steel design code EN 1993-1-4 [2] provides the following two set of equations for the design of beam-columns under axial compression plus uniaxial major axis bending moment:

$$\frac{N_{Ed}}{(N_{b,Rd})_{min}} + k_y \left(\frac{M_{y,Ed} + N_{Ed} e_{N,y}}{\beta_{w,y} W_{pl,y} f_y / \gamma_{M1}} \right) \leq 1.0, \tag{6}$$

$$\frac{N_{Ed}}{(N_{b,Rd})_{min\ 1}} + k_{LT} \left(\frac{M_{y,Ed} + N_{Ed} e_{N,y}}{M_{b,Rd}} \right) \leq 1.0 \tag{7}$$

where N_{Ed} and $M_{y,Ed}$ are the design values of the compression force and maximum moment about the major axis, $(N_{b,Rd})_{min}$ is the smallest design column buckling resistance considering flexural buckling about the major axis and minor axis, torsional buckling and torsional-flexural buckling, $(N_{b,Rd})_{min\ 1}$ is the smallest design column buckling resistance considering flexural buckling about the minor axis, torsional buckling and torsional-flexural buckling, e_{Ny} is the shift in the neutral axis when the cross-section is subjected to uniform compression, which is equal to zero for I-sections, $M_{b,Rd}$ is the lateral-torsional buckling resistance and $W_{pl,y}$ is the plastic section modulus about the major axis. In eq. (6), $\beta_{w,y}$ is an auxiliary coefficient, which is either equal to (i) 1.0 for cross-sections falling into the Class 1 and 2 categories (i.e. $\beta_{w,y} = 1.0$ for Class 1 and 2 sections), (ii) the ratio of the elastic $W_{el,y}$ to the plastic section moduli $W_{pl,y}$ about the major axis for cross-sections falling into the Class 3 category (i.e. $\beta_{w,y} = W_{el,y}/W_{pl,y}$ for Class 3 sections) or (iii) equal to the ratio of the effective $W_{eff,y}$ to the plastic section moduli $W_{pl,y}$ about the major axis for cross-sections falling into the Class 4 category (i.e. $\beta_{w,y} = W_{eff,y}/W_{pl,y}$ for Class 4 sections). In eq. (6) and eq. (7), k_y and k_{LT} are the interaction factors determined as:

$$k_y = 1 + 2\left(\overline{\lambda}_y - 0.5\right) \frac{N_{Ed}}{N_{b,Rd,y}} \quad \text{but} \quad 1.2 \leq k_y \leq 1.2 + 2\frac{N_{Ed}}{N_{b,Rd}} \tag{8}$$

$$k_{LT} = 1.0 \tag{9}$$

where $N_{b,Rd,y}$ is the major axis column flexural buckling resistance.

The accuracy of the EN 1993-1-4 [2] design provisions is assessed against the numerical and experimental results for laterally unrestrained arc-welded and laser-welded beam-columns in Fig. 10, where the design column $N_{b,Rd}$ and beam $M_{b,Rd}$ buckling resistances are determined using the existing column and beam buckling curves of EN 1993-1-4 [2]. In the figure, the ratios of the experimentally and numerically obtained ultimate strengths N_u to those determined using EN 1993-1-4 [2] $N_{u,EC3}$ (i.e. $N_u/N_{u,EC3}$) are plotted against the radial angles θ determined considering the EN 1993-1-4 [2] design interaction curves as shown in Fig. 9. The accuracy of EN 1993-1-4 [2] is also shown in Table 7. As can be seen from Fig. 10 and Table 7, EN 1993-1-4 [2] leads to somewhat overly-conservative ultimate strength predictions for laterally unrestrained stainless steel I-section beam-columns. Furthermore, owing to the lack of distinction between laser-welded members and conventionally arc-welded members, the strength predictions are more conservative for the laser-welded stainless steel beam-columns due to their lower level of residual stress.

4.3. AISC Design Guide 27 [12]

In line with the design procedure set out in AISC 360-16 [36], the following equations are given in AISC Design Guide 27 [12] for the design of stainless steel beam-columns under combined axial loading and major axis bending:

$$\frac{N_{Ed}}{N_b} + \frac{8}{9}\frac{M_{y,Ed}}{M_{y,b}} \quad \text{for} \quad \frac{N_{Ed}}{N_b} \geq 0.2 \tag{10}$$

$$\frac{N_{Ed}}{2N_b} + \frac{M_{y,Ed}}{M_{y,b}} \quad \text{for} \quad \frac{N_{Ed}}{N_b} < 0.2 \tag{11}$$

where N_b and $M_{y,b}$ are the column buckling and beam buckling resistances, determined considering both overall and local buckling effects. Note that the $P-\delta$ effects should be explicitly considered in the determination of the maximum major-axis bending moments $M_{y,Ed}$ along the lengths of stainless steel elements in the application of the beam-column design equations of AISC Design Guide 27 [12] unlike in the implementation of those given in EN 1993-1-4 [2] where the $P-\delta$ effects are considered by means of the interaction factors k_y and k_{LT}. For the case of beam-columns under axial compression plus constant major axis bending, the maximum major axis bending moment $M_{y,Ed}$ located at the mid-height of the member may be determined by amplifying the applied first order bending moments by a factor of $1/(1 - N_{Ed}/N_{cr,y})$.

An assessment of the AISC Design Guide 27 [12] design provisions is provided in Fig. 11 and Table 7. As can be seen from the figure and table, AISC Design Guide 27 [12] leads to quite scattered ultimate strength predictions for stainless steel beam-columns such that its accuracy is lower than that of EN 1993-1-4 [2]; this is largely attributed to the adopted column buckling curve.

4.4. Greiner and Kettler [13] proposal

Following the format adopted in the interaction equations of EN 1993-1-1 [37], Greiner and Kettler [13] put forward a two set of interaction equations (eqs. (12) and (13)) for the

design of laterally unrestrained stainless steel beam-columns susceptible to flexural-torsional buckling through calibration to the results from nonlinear finite element modelling:

$$\frac{N_{Ed}}{N_{b,y,Rd}} + k_{y,G\&K}\frac{M_{y,Ed}}{M_{b,Rd}} \leq 1.0, \tag{12}$$

$$\frac{N_{Ed}}{N_{b,z,Rd}} + k_{LT,G\&K}\frac{M_{y,Ed}}{M_{b,Rd}} \leq 1.0, \tag{13}$$

in which $N_{b,z,Rd}$ is the minor axis column buckling resistance considering the minor axis flexural, torsional and torsional-flexural buckling of a column, $M_{b,Rd}$ is the beam buckling resistance and $k_{G\&K,y}$ and $k_{G\&K,z}$ are the interaction factors determined as follows:

$$k_{y,G\&K} = 0.9 + 2.2(\overline{\lambda}_y - 0.4)\frac{N_{Ed}}{N_{b,y,Rd}} \quad \text{but} \quad k_{y,G\&K} \leq 0.9 + 2.42\frac{N_{Ed}}{N_{b,y,Rd}}, \tag{14}$$

$$k_{LT,G\&K} = 1 - 0.4\left(\frac{N_{Ed}}{N_{b,z,Rd}}\right)^{1.3}. \tag{15}$$

The accuracy of the method put forward by Greiner and Kettler [13] in comparison to the results from the experiments and nonlinear shell finite element modelling is illustrated in Fig. 12, as well as in Table 7, for arc-welded and laser-welded laterally unrestrained beam-columns. Note that in the application of the method of Greiner and Kettler [13], which is limited to members with Class 1 and 2 cross-sections, the column and beam buckling strengths (i.e. $N_{b,y,Rd}$, $N_{b,z,Rd}$ and $M_{b,Rd}$) were determined on the basis of the buckling curves provided in EN 1993-1-4 [2]. As can be seen from Fig. 12 and Table 7, the method put forward by Greiner and Kettler [13] leads to more accurate strength predictions relative to both EN 1993-1-4 [2] and AISC Design Guide 27 [12] for laterally unrestrained stainless steel beam-columns. However, the results remain scattered and the method is only applicable to members with Class 1 and 2 cross-sections, highlighting the need for an improved, general, consistent and accurate design method for stainless steel beam-columns.

5. New design proposal for laterally unrestrained stainless steel welded I-section beam-columns

5.1. Introduction

Aiming to achieve improved accuracy in the design of stainless steel beam-columns relative to the existing methods presented in the previous section, a new design method for laterally unrestrained stainless steel welded I-section beam-columns is proposed in this section. In line with [7, 38, 39], the general format of the beam-column interaction equations presented in EN 1993-1-1 [37] was adopted, while improvement in the accuracy of the design predictions was sought by (i) predicting more accurately the end-points of the interaction curves (i.e. the column buckling and beam buckling resistances) and (ii) calibrating new interaction factors leading to design interaction curves that more accurately reflect the ultimate strengths of stainless steel beam-columns. Focus is initially placed on the arc-welded

austenitic stainless steel beam-columns which have the more severe residual stresses relative to the laser-welded members. It is anticipated that adaptation to laser-welded members can be then achieved simply by updating the end-points, as proposed in [7]; alternatively, given that the difference between the ultimate strengths of arc-welded and laser-welded members is relatively small [7], the design provisions developed for arc-welded members could be conservatively applied to laser-welded members.

5.2. New interaction equations for stainless steel welded I-section beam-columns susceptible to flexural-torsional buckling

In accordance with the beam-column interaction equation format adopted for carbon steel members in EN 1993-1-1 [37], the following beam-column interaction formulae are proposed herein for the design laterally unrestrained I-section stainless steel beam-columns:

$$\frac{N_{Ed}}{N_{b,y,Rd}} + k_{yy,prop}\frac{M_{y,Ed}}{M_{b,Rd}} \leq 1.0 \tag{16}$$

$$\frac{N_{Ed}}{N_{b,z,Rd}} + k_{zy,prop}\frac{M_{y,Ed}}{M_{b,Rd}} \leq 1.0 \tag{17}$$

where $k_{yy,prop}$ and $k_{zy,prop}$ are the interaction factors used for the in-plane and out-of-plane buckling assessment respectively, γ_{M1} is the partial safety factor for buckling which should be taken as equal to 1.1 (i.e. $\gamma_{M1} = 1.1$) in accordance with EN 1993-1-4 [2], $N_{b,y,Rd}$ and $N_{b,z,Rd}$ are the in-plane and out-of-plane column flexural buckling strengths and $M_{b,Rd}$ is the beam lateral-torsional buckling strength. It should be noted that for the case of beam-columns with the non-dimensional lateral-torsional buckling slenderness less than or equal to 0.2 (i.e. for beam-columns with $\overline{\lambda}_{LT} \leq 0.2$), the use of cross-section bending moment resistances determined through the continuous strength method M_{csm} as described in [7] for the bending end point $M_{b,Rd}$ is recommended (i.e. $M_{b,Rd} = M_{csm}$ when $\overline{\lambda}_{lt} \leq 0.2$). The bending moment resistances $M_{b,Rd}$ can also be conservatively taken as equal to the cross-section resistances determined through the provisions of EN 1993-1-4 [2] in these cases. In the following subsections, the equations recommended for the determination of $k_{yy,prop}$, $k_{zy,prop}$, $N_{b,y,Rd}$, $N_{b,z,Rd}$ and $M_{b,Rd}$ are introduced.

5.3. Interaction factor $k_{yy,prop}$ used in in-plane buckling assessment of stainless steel beam-columns

The interaction factor $k_{yy,prop}$ used in the in-plane buckling assessment of stainless steel beam-columns is provided below:

$$k_{yy,prop} = 1 + D_{1,y}\left(\overline{\lambda}_y - D_{2,y}\right)\frac{N_{Ed}}{N_{b,y,Rd}}$$

$$\text{but} \quad k_{yy,prop} \leq 1 + D_{1,y}\left(D_{3,y} - D_{2,y}\right)\frac{N_{Ed}}{N_{b,y,Rd}}, \tag{18}$$

where $D_{1,y}$, $D_{2,y}$ and $D_{3,y}$ are the auxiliary coefficients, which have been derived in [7] through calibration against a large number of numerical and experimental results for laterally-restrained stainless steel I-section beam-columns subjected to major axis bending plus uniform compression. The values of $D_{1,y}$, $D_{2,y}$ and $D_{3,y}$ recommended in [7] are provided in

Table 8. The accuracy and reliability of using eq. (18) in conjunction with eq. (16) for the in-plane instability assessment of stainless steel beam-columns have been verified against the results obtained from physical experiments and finite element modelling for a wide range of cases in [7]. Thus eq. (18) with the $D_{1,y}$, $D_{2,y}$ and $D_{3,y}$ coefficients put forward by [7] are also adopted in this study for the determination of $k_{yy,prop}$.

5.4. Buckling resistance of welded I-section stainless steel columns

Column buckling resistances $N_{b,Rd}$ used within the interaction equations provided in eq. (16) and eq. (17) are determined by means of the equation below:

$$N_{b,Rd} = \frac{\chi A f_y}{\gamma_{M1}}, \tag{19}$$

in which χ is the buckling reduction factor determined as:

$$\chi = \frac{1}{\phi + \sqrt{\phi^2 - \overline{\lambda}^2}} \leq 1.0 \quad \text{where} \quad \phi = 0.5\left[1 + \alpha\left(\overline{\lambda} - \overline{\lambda}_0\right) + \overline{\lambda}^2\right]. \tag{20}$$

In eq. (20), $\overline{\lambda}_0$ is the plateau slenderness for column buckling below which $\chi = 1.0$ and α is the imperfection factor, values for which are provided in Table 9 for the major axis (i.e. in-plane) and minor axis (i.e. out-of-plane) buckling of arc-welded and laser-welded stainless steel I-section columns. Note that the α and $\overline{\lambda}_0$ values provided in Table 9 for laser-welded columns were obtained through calibration against the results from physical experiments and nonlinear finite element modelling in [8]. The values of α and $\overline{\lambda}_0$ given in Table 9 for conventionally arc-welded columns are the same as those provided in EN 1993-1-4 [2]; the suitability of these values was also confirmed in [8].

5.5. Lateral-torsional buckling resistance of welded I-section stainless steel beams

The lateral-torsional buckling (LTB) strengths of stainless steel beams $M_{b,Rd}$, which are utilised in eq. (17), are calculated using the following equation:

$$M_{b,Rd} = \frac{\chi_{LT} W_y f_y}{\gamma_{M1}}, \tag{21}$$

in which W_y is the plastic $W_{pl,y}$, elastic $W_{el,y}$ or effective $W_{eff,y}$ section modulus about the major axis depending on the class of a cross-section according to [2] and χ_{LT} is the LTB reduction factor. For the determination of χ_{LT}, the use of the following expression, which was originally put forward by Taras and Greiner [40] for carbon steel beams and is due to be incorporated into the upcoming version of EN 1993-1-1 [37] (currently referred to as prEN 1993-1-1 [41]), is recommended:

$$\chi_{LT} = \frac{1}{\phi_{LT} + \sqrt{\phi_{LT}^2 - \overline{\lambda}_{LT}^2}} \leq 1.0$$

$$\text{where} \quad \phi_{LT} = 0.5\left[1 + \alpha_{LT}\left(\overline{\lambda}_z - 0.2\right)\left(\frac{\overline{\lambda}_{LT}}{\overline{\lambda}_z}\right)^2 + \overline{\lambda}_{LT}^2\right] \tag{22}$$

where α_{LT} is the imperfection factor for LTB which should be taken as equal to $\alpha_{LT} = 0.21\sqrt{W_{el,y}/W_{el,z}} \leq 0.64$ as recommended for I-sections in prEN 1993-1-1 [41], $W_{el,z}$ is the elastic section modulus about the minor axis and $\overline{\lambda}_z$ is the non-dimensional slenderness for flexural buckling about the minor axis.

In Fig. 13 (a), the accuracy of the LTB assessment equation provided in prEN 1993-1-1 [41] is assessed against the GMNIA results of fork-end supported arc-welded austenitic stainless steel beams subjected to uniform bending with cross-section depth $h = 50$ mm and cross-section aspect ratios equal to 1.0, 1.5, 2.0 and 3 (i.e. h/b_f=1.0, 1.5, 2.0, 3.0). Three different flange t_f and web thickness t_w values were selected for the each considered aspect ratio, resulting in twelve different cross-section profiles covering Class 1, 2 and 3 according to EN 1993-1-4 [2]; the t_f and t_w values were selected such that the non-dimensional plate buckling slendernesses for flange and web plates were the same (i.e. $\overline{\lambda}_{p,f} = \overline{\lambda}_{p,w}$). Fig. 13 (a) shows that the LTB assessment equation provided in prEN 1993-1-1 [41], originally developed for welded carbon steel beams, provides very accurate ultimate strength predictions also for welded austenitic stainless steel beams. Thus, the adoption of this equation for the design of austenitic stainless steel beams against LTB is recommended in this paper. The accuracy of the LTB curve given in EN 1993-1-4 [2] is assessed in Fig. 13 (b), showing that EN 1993-1-4 [2] leads to less accurate LTB strength predictions for austenitic stainless steel beams.

Assessment of the prEN 1993-1-1 [41] and EN 1993-1-4 [2] provisions for the LTB strength predictions of fork-end supported arc-welded austenitic stainless steel I-section beams subjected to uniform bending is also provided in Table 10, where S is the ratio of the ultimate strength determined by GMNIA to that obtained from the design methods (i.e. $S = M_{ult,FE}/M_{b,Rd}$); S_{av}, S_{cov}, S_{max} and S_{min} are the average, coefficient of variation, maximum and minimum values of S for the considered beams in the table. Table 10 shows that prEN 1993-1-1 [41] leads to considerably more accurate LTB strength predictions relative to EN 1993-1-4 [2] for austenitic stainless steel beams.

5.6. Derivation of interaction factor $k_{zy,prop}$ used in out-of-plane buckling assessment of stainless steel beam-columns

Upon the establishment of the flexural buckling and lateral-torsional buckling assessment equations for welded I-section stainless steel members, an expression for the interaction factor $k_{zy,prop}$ for the out-of-plane buckling assessment of stainless steel beam-columns subjected to axial compression plus major axis bending is developed in this subsection. In line with EN 1993-1-1 [37], the following format of equation is recommended in this paper for the determination of the interaction factor $k_{zy,prop}$:

$$k_{zy,prop} = 1 - \frac{D_{1,LT}\overline{\lambda}_z \frac{N_{Ed}}{N_{b,z,Rd}}}{1 - D_{2,LT}} \qquad \text{but} \qquad k_{zy,prop} \leq 1 - \frac{D_{1,LT}D_{3,LT}\frac{N_{Ed}}{N_{b,z,Rd}}}{1 - D_{2,LT}} \tag{23}$$

where $D_{1,LT}$, $D_{2,LT}$ and $D_{3,LT}$ are the auxiliary coefficients. The interaction factor $k_{zy,prop}$ is calibrated herein against the numerically-derived interaction factors $k_{zy,FE}$, the values of which were determined from eq. (24), which is a rearrangement of eq. (17) in terms of

$k_{zy,prop}$:

$$k_{zy,FE} = \left(1 - \frac{N_{u,FE}}{N_{b,z,Rd}}\right) \frac{M_{b,Rd}}{M_{y,u,FE}}. \tag{24}$$

where $N_{u,FE}$ and $M_{y,u,FE}$ are the ultimate axial loads and major axis bending moments obtained through GMNIA of the stainless steel beam-columns and $N_{b,z,Rd}$ and $M_{b,Rd}$ are the minor axis flexural buckling and lateral-torsional buckling resistances of the beam-columns determined using eq. (20) and eq. (22), respectively.

During the calibration of $k_{zy,prop}$, it was observed that the values of the numerically-generated out-of-plane interaction factors $k_{zy,FE}$ were dependent upon the cross-section shape. For the case of beam-columns with Class 3 sections, the highest $k_{zy,FE}$ values were achieved for the cross-sections with the lowest aspect ratios (i.e. h/b_f values), whereas for the case of beam-columns with Class 1 sections, the reverse was true. However, following the same approach used by Greiner and Lindner [28, 29] in the calibration of the EN 1993-1-1 [37] beam-column interaction factors, safe-sided values for the auxiliary coefficients $D_{1,LT}$, $D_{2,LT}$ and $D_{3,LT}$ are proposed herein based on the upper bound numerically-generated $k_{zy,FE}$ values, as given in Table 11. Comparisons between the numerically-generated $k_{zy,FE}$ values and the proposed $k_{zy,prop}$ values for austenitic stainless steel beam-columns with different cross-section shapes are given in Fig. 14, where n_z is the ratio of the applied axial load N_{Ed} to the minor axis flexural buckling resistance $N_{b,z,Rd}$ of the member (i.e. $n_z = N_{Ed}/N_{b,z,Rd}$). Note that, as in previous research [7, 38], calculated resistances were used as the end points in the derivation of the interaction factors, though similar results (following reliability analysis) would be expected if numerical resistances had been used.

The accuracy of the proposals for arc-welded and laser-welded stainless steel beam-columns subjected to axial compression plus uniform major axis bending is assessed in Fig. 15 and Table 12, considering the numerical GMNIA results generated herein in Section 3.5, as well as the experimental results of [9, 11, 34] for arc-welded austenitic stainless steel beam-columns and the experimental results presented in the current paper and in [5] for laser-welded austenitic stainless steel beam-columns. Fig. 15 and Table 12 show that the proposed design approach generally leads to accurate and safe-sided ultimate resistance predictions for both arc-welded and laser-welded stainless steel beam-columns. As can be seen by comparing Table 12 and Table 7, the values of ϵ_{cov} obtained through the proposed approach are smaller than those determined through all the existing design approaches (i.e. EN 1993-1-4 [2], AISC Design Guide 27 [12] and the proposal of Greiner and Kettler [13]), indicating more consistent resistance predictions. Furthermore, the ϵ_{av} values are closer to 1.0, indicating that the proposed approach is more accurate than the existing methods for the design of austenitic stainless steel beam-columns. In the following subsection, the reliability of the presented design proposals for austenitic stainless steel beam-columns is assessed.

6. Reliability analysis

In this section, the reliability of the proposed approach for the design of austenitic stainless steel beam-columns is assessed following the procedure given in Annex D of EN 1990 [42], on the basis of the experimental and numerical results generated in this paper and the experimental results provided in [7, 9–11]. The key parameters from the reliability analysis are shown in Table 13, in which N is the number of experimental and numerical data taken into consideration, b is the mean value correction factor, $k_{d,n}$ is the fractile factor which is dependent upon the number of the data considered and V_δ is the coefficient of variation of the experimental and numerical ultimate strengths relative to the resistance prediction. Note that the mean correction factor b was determined herein by taking the average of the ratios of the experimental and numerical ultimate resistances to those predicted by the proposed design method; unlike the least squares approach recommended in EN 1990 [42], this avoids the bias of b towards the experimental or numerical results with larger ultimate resistances [43, 44]. In accordance with the recommendations provided in [43], the material overstrength factor, defined as the ratio of the mean yield strength $f_{y,mean}$ to the nominal yield strength $f_{y,nom}$, was taken as $f_{y,mean}/f_{y,nom} = 1.30$, while the coefficients of variation of the yield strength V_{fy} and geometry $V_{geometry}$ were taken as 0.06 and 0.05 respectively (i.e. $V_{fy} = 0.06$ and $V_{geometry} = 0.05$). Table 13 shows that the determined partial safety factors γ_{M1} are lower than or very close to the partial safety factor value of $\gamma_{M1} = 1.10$ recommended in EN 1993-1-4 [2], indicating that the proposed method can be safely used for the design of austenitic stainless steel beam-columns susceptible to flexural-torsional buckling.

7. Summary of the design recommendations for codification

In this section, a summary of the proposals for the design of stainless steel beam-columns is presented, based both on the research presented in this paper and other recent research studies carried out within the steel structures research group at Imperial College London [7, 38, 45]. In addition to the design proposals presented herein for stainless steel I-section beam-columns susceptible to flexural-torsional buckling, the following are also collated from the literature: (i) the design proposals of [7] for laterally restrained stainless steel I-section beam-columns subjected to major axis bending plus axial compression and minor axis bending plus axial compression, (ii) the recommendations of [38] for the design of stainless steel beam-columns with square hollow sections (SHS) and rectangular hollow sections (RHS) and (iii) the design method of [45] for stainless steel beam-columns with circular hollow sections (CHS). This covers the majority of the commonly employed cross-section types in practice. For SHS, RHS and CHS beam-columns, interaction expressions have been developed for austenitic, duplex and ferritic stainless steel members [38, 45]. However, for I-section beam-columns, only austenitic stainless steel has been explored thus far. The proposals made herein though would be expected to provide safe-sided strength predictions for duplex and ferritic stainless steel I-section beam-columns owing to the lower degree of nonlinearity in the material response of these grades compared to that of austenitic stainless steel. Further

research is currently underway to develop specific proposals for duplex and ferritic stainless steel I-section beam-columns.

Adopting the interaction equation format of prEN 1993-1-1 [41] to bring consistency with carbon steel design, the following set of equations are recommended for the design of stainless steel beam-columns:

$$\frac{N_{Ed}}{\chi_y \frac{N_{Rk}}{\gamma_{M1}}} + k_{yy}\frac{M_{y,Ed}+\Delta M_{y,Ed}}{\chi_{LT}\frac{M_{y,Rk}}{\gamma_{M1}}} + k_{yz}\frac{M_{z,Ed}+\Delta M_{z,Ed}}{\frac{M_{z,Rk}}{\gamma_{M1}}} \leq 1.0 \tag{25}$$

$$\frac{N_{Ed}}{\chi_z \frac{N_{Rk}}{\gamma_{M1}}} + k_{zy}\frac{M_{y,Ed}+\Delta M_{y,Ed}}{\chi_{LT}\frac{M_{y,Rk}}{\gamma_{M1}}} + k_{zz}\frac{M_{z,Ed}+\Delta M_{z,Ed}}{\frac{M_{z,Rk}}{\gamma_{M1}}} \leq 1.0 \tag{26}$$

where N_{Ed} is the design value of the compression force and $M_{y,Ed}$ and $M_{z,Ed}$ are the design values of the maximum bending moments about the y-y and z-z axes along the member, N_{Rk}, $M_{y,Rk}$ and $M_{z,Rk}$ are the characteristic values of the cross-sectional resistance to compressive axial force and bending moments about the y-y and z-z axes respectively, γ_{M1} is the partial factor for the resistance of members to instability assessed by member checks, taken as $\gamma_{M1} = 1.10$, $\Delta M_{y,Ed}$ and $\Delta M_{z,Ed}$ are the moments due to the shift of the centroid axis for Class 4 sections, χ_y and χ_z are the flexural buckling reduction factors from eq. (20) using the corresponding α and $\overline{\lambda}_0$ values for I-sections from Table 9 and those for CHS, SHS and RHS from [38, 45], χ_{LT} is the lateral torsional buckling reduction factor from eq. (22) and k_{yy}, k_{yz}, k_{zy}, and k_{zz} are the interaction factors.

The characteristic resistance to axial force N_{Rk} is determined using the following equations as set out in EN 1993-1-4 [2]:

$$N_{Rk} = Af_y \quad \text{for} \quad \text{Class 1, 2 or 3 section}$$
$$N_{Rk} = A_{eff}f_y \quad \text{for} \quad \text{Class 4 section}$$

in which A and A_{eff} are the full and effective cross-section areas, respectively. In eq. (25) and eq. (26), the characteristic moment resistances $M_{y,Rk}$ and $M_{z,Rk}$ may be calculated according to the Continuous Strength Method (CSM) [46, 47] for I-sections, SHS, RHS and CHS cross-sections as described in [7, 38, 45], provided the non-dimensional LTB slenderness of the stainless steel beam-column $\overline{\lambda}_{LT}$ is less than the threshold value of $\overline{\lambda}_{LT,0} = 0.4$, which indicates that the member is not susceptible to flexural-torsional buckling as stated in [41]:

$$M_{y,Rk} = M_{y,csm} \quad \text{and} \quad M_{z,Rk} = M_{z,csm} \quad \text{for} \quad \overline{\lambda}_{LT} \leq \overline{\lambda}_{LT,0} = 0.4 \tag{27}$$

where $M_{y,csm}$ and $M_{z,csm}$ are the major and minor axis bending moment resistances, respectively, calculated according to the CSM. Alternatively for $\overline{\lambda}_{LT} \leq \overline{\lambda}_{LT,0}$ and in all cases when $\overline{\lambda}_{LT} > \overline{\lambda}_{LT,0} = 0.4$, the characteristic moment resistances $M_{y,Rk}$ and $M_{z,Rk}$ may be determined using the following expressions:

$$M_{y,Rk} = W_{pl,y}f_y \quad \text{and} \quad M_{z,Rk} = W_{pl,z}f_y \quad \text{for Class 1 and 2 sections}$$
$$M_{y,Rk} = W_{el,y}f_y \quad \text{and} \quad M_{z,Rk} = W_{el,z}f_y \quad \text{for Class 3 sections}$$
$$M_{y,Rk} = W_{eff,y}f_y \quad \text{and} \quad M_{z,Rk} = W_{eff,z}f_y \quad \text{for Class 4 sections} \tag{28}$$

in which $W_{pl,z}, W_{el,z}$ and $W_{eff,z}$ are the plastic, elastic and effective section moduli about the z-z axis.

Finally, the interaction factors k_{yy}, k_{yz}, k_{zy}, and k_{zz} employed in eq. (25) and (26) should be calculated using Table 14 and Table 15. It is currently recommended that the moment gradient factors C_{my}, C_{mz} and C_{mLT} should be determined as described in prEN 1993-1-1 [41] for carbon steel beam-columns though further research is underway on this topic. Note that the moment gradient factors C_m set out in prEN 1993-1-1 [41] for beam-columns under unequal end-moments were originally derived considering the elastic buckling response of members [29], and shown to provide safe and accurate resistance predictions when incorporated into the interaction factor expressions for steel beam-columns experiencing plasticity [29]. In [39], it was also illustrated that use of these elastically-derived C_m factors in the interaction factor expressions originally derived for SHS and RHS stainless steel beam-columns under uniform bending also leads to safe and accurate ultimate strength predictions for those under moment gradients. Given their elastic (i.e. material independent) origins and their successful application to stainless steel SHS and RHS beam-columns, it is anticipated that the use of the moment gradient factors provided in prEN 1993-1-1 [41] in the interaction factor expressions derived herein for stainless steel I-section beam-columns under uniform bending would also lead to safe and accurate results under moment gradients. However, since further research is necessary to verify this, an explanatory note for the relevant interaction factor expressions in Table 14 and Table 15 is provided. The parameters n_y and n_z used in Table 14 and Table 15 are calculated using the equations below:

$$n_y = \frac{N_{Ed}}{\chi_y N_{Rk}/\gamma_{M1}} \qquad n_z = \frac{N_{Ed}}{\chi_z N_{Rk}/\gamma_{M1}}. \tag{29}$$

For cross-section types not addressed herein (e.g. angles, channels and lipped channels), use of the beam-column design approach provided in EN 1993-1-3 [48] is recommended.

8. Conclusions

The flexural-torsional buckling response of austenitic stainless steel I-section beam-columns has been investigated both experimentally and numerically in this paper. Initially, five laboratory tests were carried out on laser-welded stainless steel beam-columns subjected to axial compression with different loading eccentricities, thus subjecting the specimens to different levels of axial compression and major axis bending moments. A detailed description of the test setup, experimental procedure, specimen properties and test results has been presented. Finite element models of austenitic stainless steel I-section beam-columns were created and validated against the experimental results. Parametric studies were then carried out on both conventionally arc-welded and laser-welded austenitic stainless steel members considering their different levels of residual stress; a range of the cross-section dimensions, member slendernesses and loading conditions was examined. It was observed that the laser-welded stainless steel beam-columns possess higher ultimate load carrying capacities relative to the arc-welded stainless steel beam-columns due to the presence of lower residual stresses in the former. On the basis of the results obtained from the numerical parametric studies,

as well as the physical tests carried out both in this paper and collected from the literature [9, 11, 34], the accuracy and safety of the methods provided in the European structural stainless steel design code EN 1993-1-4 [2], the American Institute of Steel Construction (AISC) Design Guide 27 [12] and the approach proposed by Greiner and Kettler [13] for the design of stainless steel beam-columns were assessed. It was observed that EN 1993-1-4 [2] yields safe-sided but rather conservative ultimate strength predictions for austenitic stainless steel beam-columns susceptible to flexural-torsional buckling, while the design method provided in AISC Design Guide 27 [12] provides less conservative and more scattered ultimate strength predictions. Relative to EN 1993-1-1 [2] and AISC Design Guide 27 [12], the method of Greiner and Kettler [13] provides more accurate ultimate strength predictions, though further scope for improvement was still observed. Thus, on the basis of the results from the numerical parametric studies together with the new and existing experiments, a new design method leading to more accurate design predictions relative to the existing design methods [2, 12, 13] for austenitic stainless steel beam-columns was developed. Verification of the reliability of the new proposed design method in accordance with the procedure given in EN 1990 [42] is illustrated. A summary of the design proposals set out in this paper and from the recent research carried out in [38, 45] is also provided. The approach proposed in this paper for the design of austenitic stainless steel beam-columns is consistent with the approach for carbon steel in EN 1993-1-1 [37] and is expected to be incorporated into the upcoming version of the European structural stainless steel design code EN 1993-1-4 [2].

References

[1] Gardner, L.. Stability and design of stainless steel structures–Review and outlook. Thin-Walled Structures 2019;141:208–216.

[2] EN 1993-1-4, Eurocode 3 Design of steel structures-Part 1-4: General rules – Supplementary rules for stainless steel. European Committee for Standardization (CEN), Brussels; 2015.

[3] SEI/ASCE 8-02, Specification for the design of cold-formed stainless steel structural members. American Society of Civil Engineers (ASCE), Reston, Virginia, USA; 2001.

[4] AS/NZS 4673, Cold-formed stainless steel structures. Standard, Australian and Standard, New Zealand; 2001.

[5] Gardner, L., Bu, Y., Theofanous, M.. Laser-welded stainless steel I-sections: Residual stress measurements and column buckling tests. Engineering Structures 2016;127:536–548.

[6] Bu, Y., Gardner, L.. Local stability of laser-welded stainless steel I-sections in bending. Journal of Constructional Steel Research 2018;148:49–64.

[7] Bu, Y., Gardner, L.. Laser-welded stainless steel I-section beam-columns: Testing, simulation and design. Engineering Structures 2019;179:23–36.

[8] Bu, Y., Gardner, L.. Finite element modelling and design of welded stainless steel I-section columns. Journal of Constructional Steel Research 2019;152:57–67.

[9] Yang, L., Zhao, M., Gardner, L., Ning, K., Wang, J.. Member stability of stainless steel welded I-section beam-columns. Journal of Constructional Steel Research 2019;155:33–45.

[10] Zheng, B., Hua, X., Shu, G.. Tests of cold-formed and welded stainless steel beam-columns. Journal of Constructional Steel Research 2015;111:1–10.

[11] Burgan, B., Baddoo, N., Gilsenan, K.. Structural design of stainless steel members—comparison between Eurocode 3, Part 1.4 and test results. Journal of Constructional Steel Research 2000;54(1):51–73.

[12] AISC Design Guide 27: Structural Stainless Steel. American Institute of Steel Construction (AISC), Chicago, Illinois, USA; 2013.
[13] Greiner, R., Kettler, M.. Interaction of bending and axial compression of stainless steel members. Journal of Constructional Steel Research 2008;64(11):1217–1224.
[14] EN ISO 6892-1. Metallic materials-Tensile testing-Part 1: Method of test at room temperature. European Committee for Standardization (CEN), Brussels; 2009.
[15] Mirambell, E., Real, E.. On the calculation of deflections in structural stainless steel beams: an experimental and numerical investigation. Journal of Constructional Steel Research 2000;54(1):109–133.
[16] Gardner, L., Ashraf, M.. Structural design for non-linear metallic materials. Engineering Structures 2006;28(6):926–934.
[17] Arrayago, I., Real, E., Gardner, L.. Description of stress–strain curves for stainless steel alloys. Materials & Design 2015;87:540–552.
[18] Ziemian, R.D.. Guide to stability design criteria for metal structures. John Wiley & Sons; 2010.
[19] Tebedge, N., Alpsten, G., Tall, L.. Residual-stress measurement by the sectioning method. Experimental Mechanics 1973;13(2):88–96.
[20] Klopper, J., Laubscher, R., Steuwer, A., James, M.. An investigation into the effect of weld technique on the residual stress distribution of 3CR12 (DIN 1.4003) built-up structural sections. Proceedings of the Institution of Mechanical Engineers, Part L: Journal of Materials: Design and Applications 2011;225(3):123–132.
[21] Yuan, H., Wang, Y., Shi, Y., Gardner, L.. Residual stress distributions in welded stainless steel sections. Thin-Walled Structures 2014;79:38–51.
[22] Schafer, B., Peköz, T.. Computational modeling of cold-formed steel: characterizing geometric imperfections and residual stresses. Journal of constructional steel research 1998;47(3):193–210.
[23] Abaqus 2018 Reference Manual. Simulia, Dassault Systemes; 2018.
[24] Kucukler, M., Gardner, L., Macorini, L.. Lateral–torsional buckling assessment of steel beams through a stiffness reduction method. Journal of Constructional Steel Research 2015;109:87–100.
[25] Kucukler, M., Gardner, L., Macorini, L.. Flexural–torsional buckling assessment of steel beam–columns through a stiffness reduction method. Engineering Structures 2015;101:662–676.
[26] Kucukler, M., Gardner, L.. Design of web-tapered steel beams against lateral-torsional buckling through a stiffness reduction method. Engineering Structures 2019;190:246–261.
[27] Boissonnade, N., Jaspart, J.P., Muzeau, J.P., Villette, M.. New interaction formulae for beam-columns in Eurocode 3: The French–Belgian approach. Journal of Constructional Steel Research 2004;60(3-5):421–431.
[28] Greiner, R., Lindner, J.. Interaction formulae for members subjected to bending and axial compression in Eurocode 3—the Method 2 approach. Journal of Constructional Steel Research 2006;62(8):757–770.
[29] Boissonnade, N., Greiner, R., Jaspart, J.P., Lindner, J.. Rules for Member Stability in EN 1993-1-1: Background documentation and design guidelines, Publication No. 119. European Convention for Constructional Steelwork (ECCS); 2006.
[30] EN 1990-2, Execution of Steel Structures and Aluminium Structures-Part 2: Technical Requirements for Steel Structures. European Committee for Standardization (CEN), Brussels; 2008.
[31] EN 1993-1-5, Eurocode 3 Design of steel structures-Part 1-5: Plated structural elements. European Committee for Standardization (CEN), Brussels; 2005.
[32] Jandera, M., Gardner, L., Machacek, J.. Residual stresses in cold-rolled stainless steel hollow sections. Journal of Constructional Steel Research 2008;64(11):1255–1263.
[33] Afshan, S., Zhao, O., Gardner, L.. Standardised material properties for numerical parametric studies of stainless steel structures and buckling curves for tubular columns. Journal of Constructional Steel Research 2019;152:2–11.
[34] Wang, Y., Yang, L., Gao, B., Shi, Y., Yuan, H.. Experimental study of lateral-torsional buckling behavior of stainless steel welded I-section beams. International Journal of Steel Structures 2014;14(2):411–420.

[35] Yang, L., Zhao, M., Chan, T.M., Shang, F., Xu, D.. Flexural buckling of welded austenitic and duplex stainless steel I-section columns. Journal of Constructional Steel Research 2016;122:339–353.
[36] AISC-360-16, Specifications for structural steel buildings. Chicago; 2016.
[37] EN 1993-1-1, Eurocode 3 Design of steel structures-Part 1-1: General rules and rules for buildings. European Committee for Standardization (CEN), Brussels; 2005.
[38] Zhao, O., Gardner, L., Young, B.. Behaviour and design of stainless steel SHS and RHS beam-columns. Thin-Walled Structures 2016;106:330–345.
[39] Zhao, O., Gardner, L., Young, B.. Finite element modelling and design of stainless steel SHS and RHS beam-columns under moment gradients. Thin-Walled Structures 2019;134:220–232.
[40] Taras, A., Greiner, R.. New design curves for lateral–torsional buckling—Proposal based on a consistent derivation. Journal of Constructional Steel Research 2010;66(5):648–663.
[41] prEN 1993-1-1, Final Draft of Eurocode 3 Design of steel structures-Part 1-1: General rules and rules for buildings. European Committee for Standardization (CEN), Brussels; 2018.
[42] EN 1990, Basis for structural design. European Committee for Standardization (CEN), Brussels; 2005.
[43] Afshan, S., Francis, P., Baddoo, N., Gardner, L.. Reliability analysis of structural stainless steel design provisions. Journal of Constructional Steel Research 2015;114:293–304.
[44] Meng, X., Gardner, L.. Simulation and design of semi-compact elliptical hollow sections. Engineering Structures 2019;Submitted for publication.
[45] Buchanan, C., Zhao, O., Real, E., Gardner, L.. Testing, FE modelling and design of stainless steel CHS beam-columns. Thin-Walled Structures 2019;Submitted for publication.
[46] Gardner, L.. The continuous strength method. Proceedings of the Institution of Civil Engineers-Structures and Buildings 2008;161(3):127–133.
[47] Afshan, S., Gardner, L.. The continuous strength method for structural stainless steel design. Thin-Walled Structures 2013;68:42–49.
[48] EN 1993-1-3, Eurocode 3 Design of steel structures-Part 1-3: General rules – Supplementary rules for cold-formed members and sheeting. European Committee for Standardization (CEN), Brussels; 2009.

Figures captions

Figure 1 : Generic residual stress pattern utilised for welded-sections (+ve = tension, -ve = compression)

Figure 2 : Test configuration

Figure 3 : Configuration of strain potentiometers and strain gauges used to measure deformations and strains at the mid-height of the specimens

Figure 4 : Failure modes of the specimens, featuring flexural-torsional buckling

Figure 5 : Load versus deformation curves obtained through physical laboratory tests and nonlinear finite element modelling

Figure 6 : Load versus mid-height strain curves obtained through physical laboratory tests and nonlinear finite element modelling

Figure 7 : Examples of global and local buckling modes used to define geometric imperfections in finite element models

Figure 8 : Comparison between experimental and numerical failure modes

Figure 9 : Means of assessment of different design methods against the results obtained from the physical tests or finite element (FE) models

Figure 10 : Assessment of EN 1993-1-4 design provisions for conventionally arc-welded and laser-welded beam-columns

Figure 11 : Assessment of AISC Design Guide 27 [12] design provisions for conventionally arc-welded and laser-welded beam-columns

Figure 12 : Assessment of Greiner and Kettler [13] design provisions for conventionally arc-welded and laser-welded beam-columns

Figure 13 : Accuracy assessment of the LTB assessment equations given in prEN 1993-1-1 [41] and EN 1993-1-4 [2] for arc-welded stainless steel beams under uniform bending

Figure 14 : Comparison of the proposed interaction factors $k_{zy,prop}$ against the numerically-determined interaction factors $k_{zy,FE}$ for austenitic stainless steel beam-columns with different cross-sections

Figure 15 : Accuracy of the proposals for the ultimate resistance predictions of arc-welded and laser-welded austenitic stainless steel beam-columns susceptible to flexural-torsional buckling

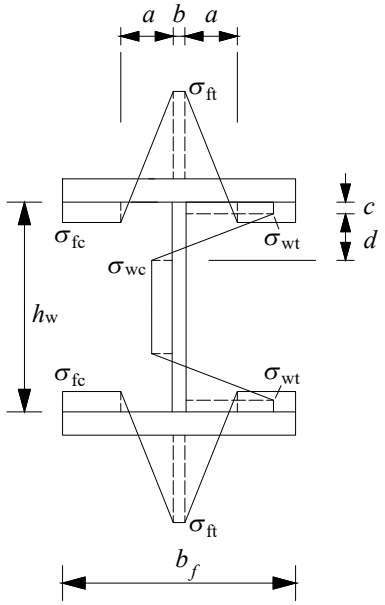

Figure 1: Generic residual stress pattern utilised for welded-sections (+ve = tension, -ve = compression)

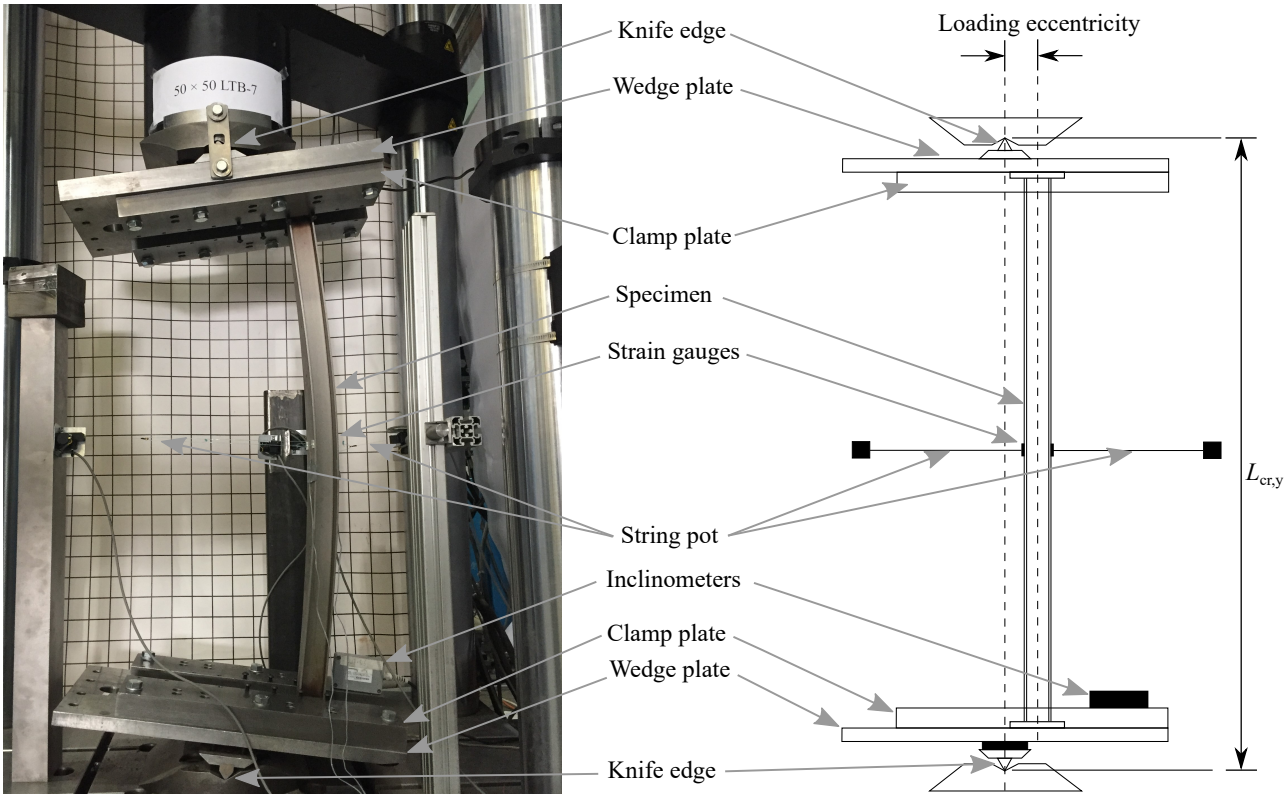

Figure 2: Test configuration

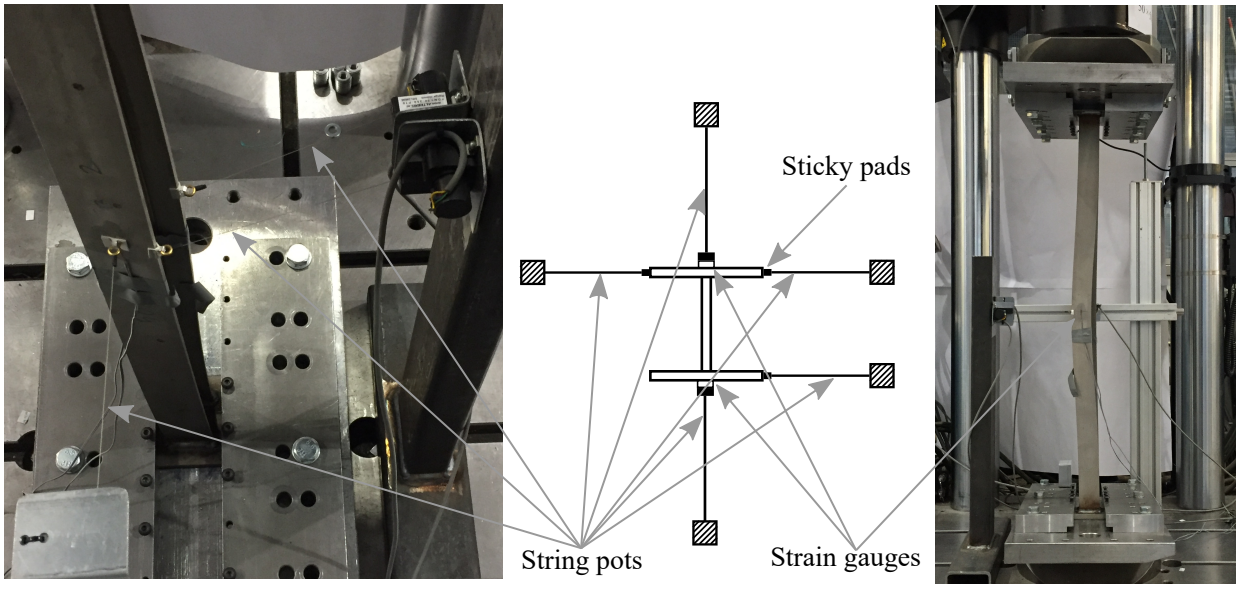

Figure 3: Configuration of strain potentiometers and strain gauges used to measure deformations and strains at the mid-height of the specimens

(a) Front view

(b) Side view

Figure 4: Failure modes of the specimens, featuring flexural-torsional buckling

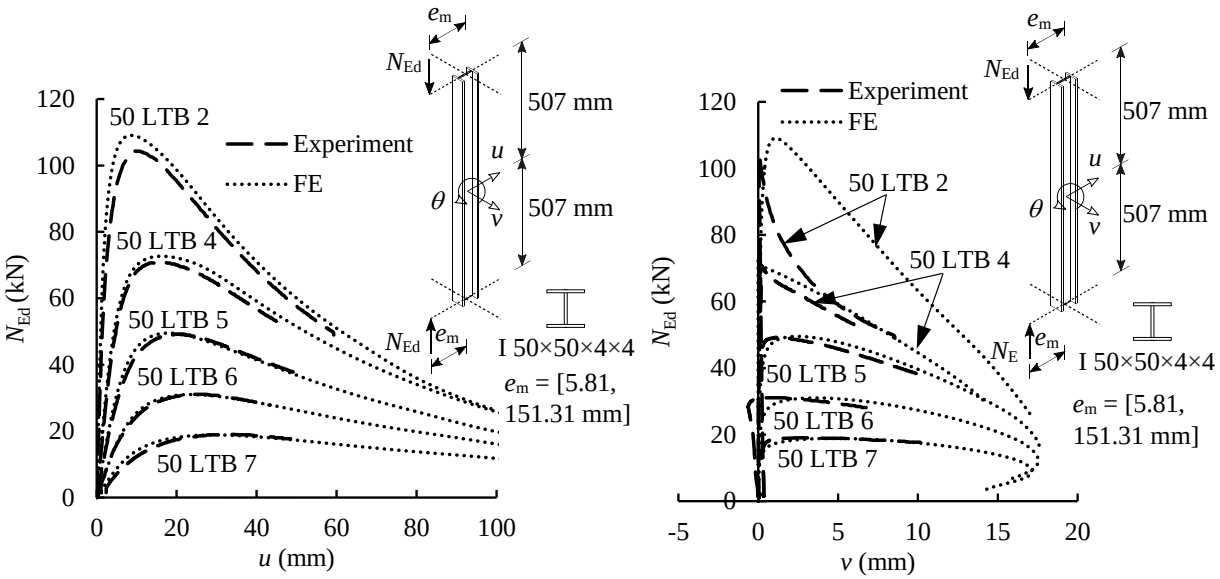

(a) Load vs mid-height in-plane deformation

(b) Load vs mid-height out-of-plane deformation

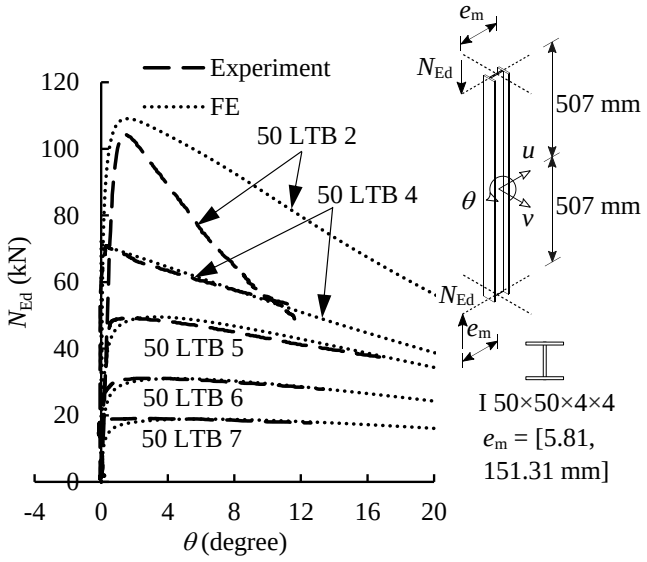

(c) Load vs mid-height twist deformation

Figure 5: Load versus deformation curves obtained through physical laboratory tests and nonlinear finite element modelling

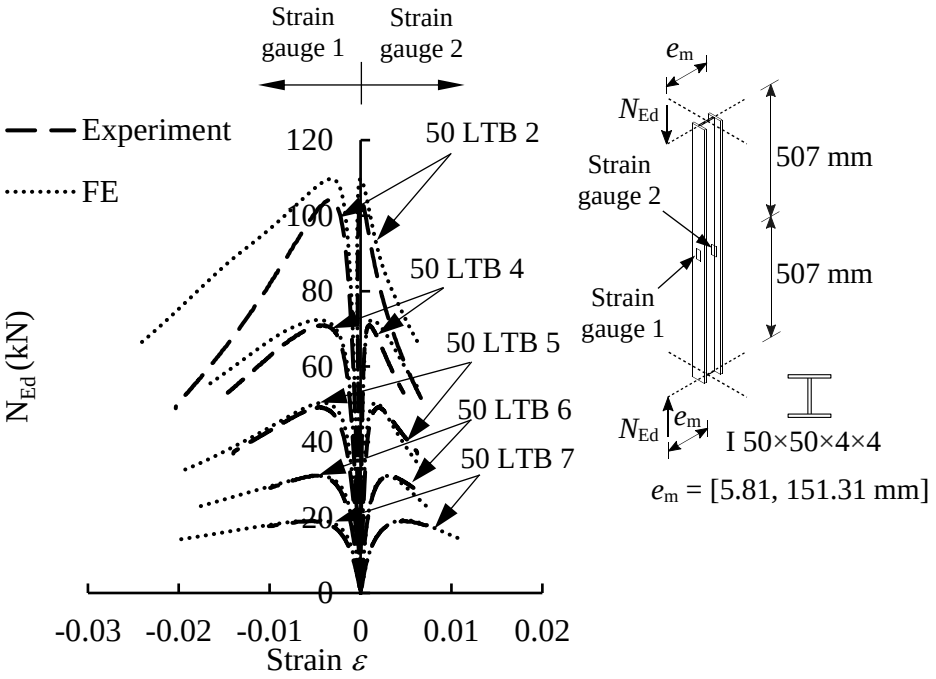

Figure 6: Load versus mid-height strain curves obtained through physical laboratory tests and nonlinear finite element modelling

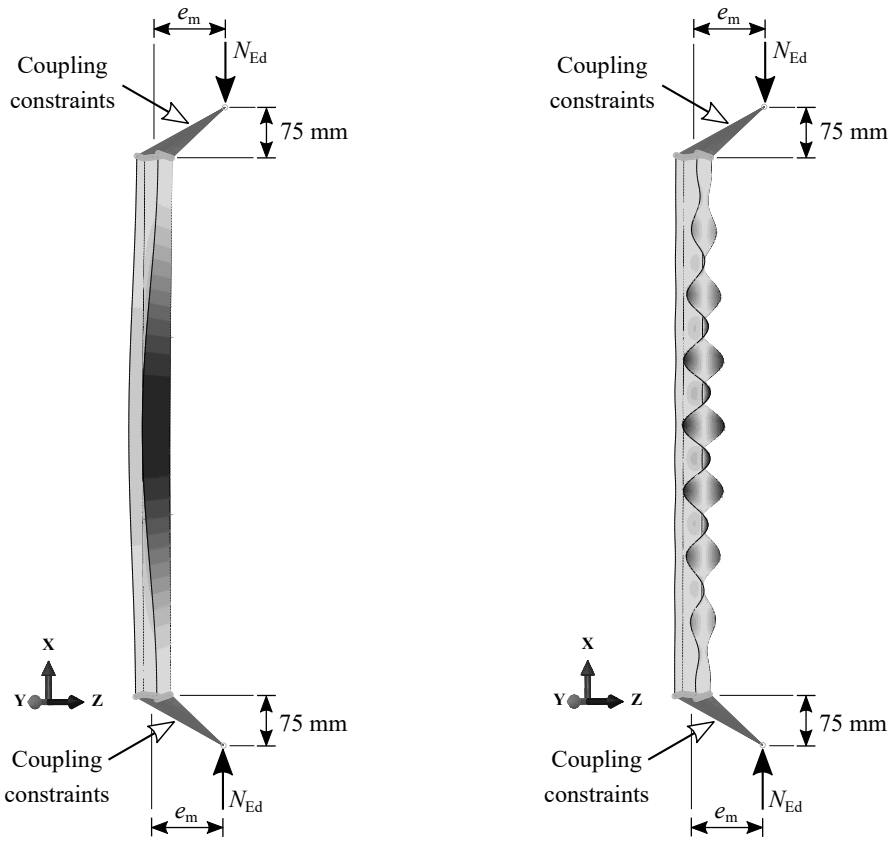

(a) Global buckling mode

(b) Local buckling mode

Figure 7: Examples of global and local buckling modes used to define geometric imperfections in finite element models

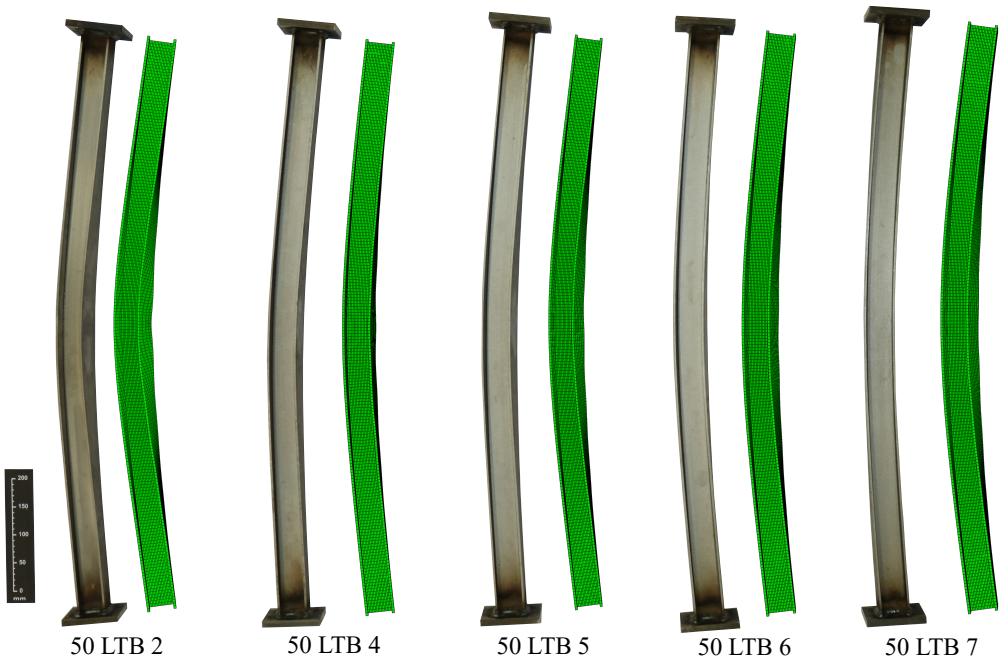

(a) Side view

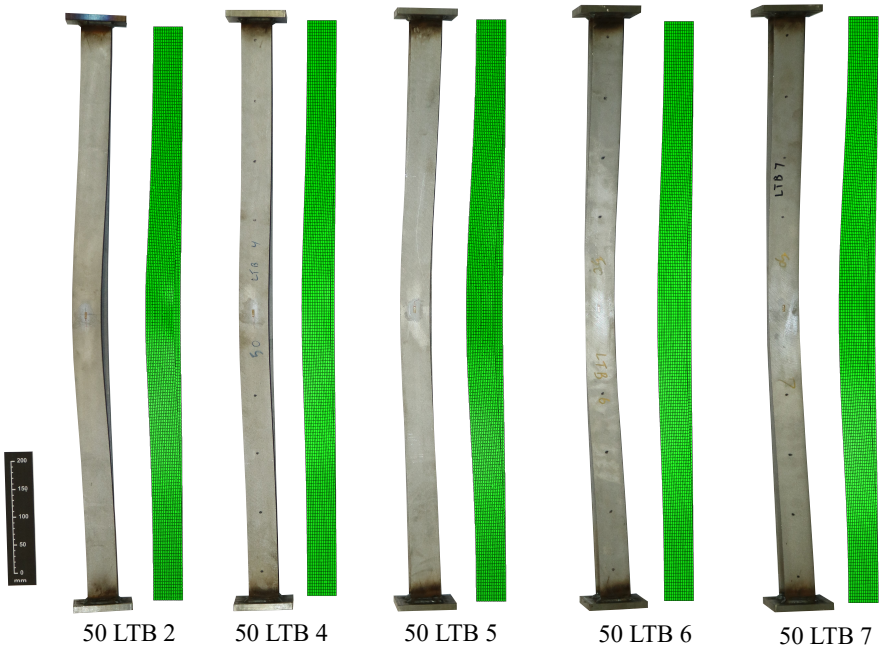

(b) Front view

Figure 8: Comparison between experimental and numerical failure modes

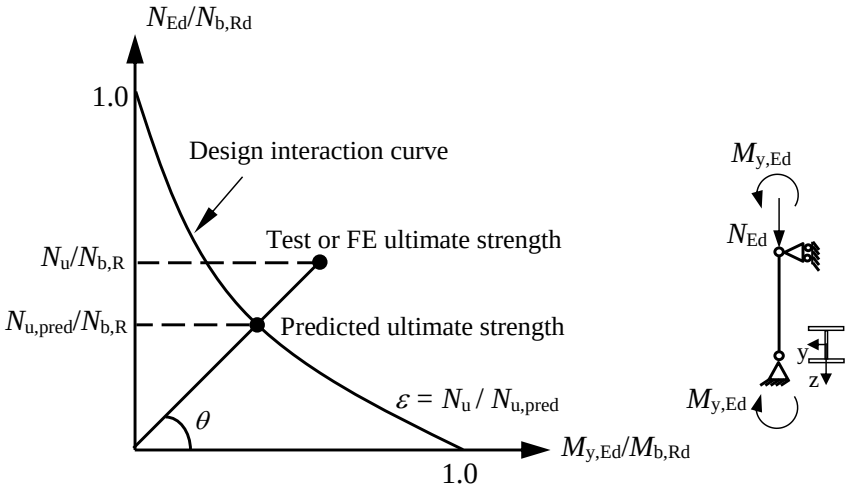

Figure 9: Means of assessment of different design methods against the results obtained from the physical tests or finite element (FE) models

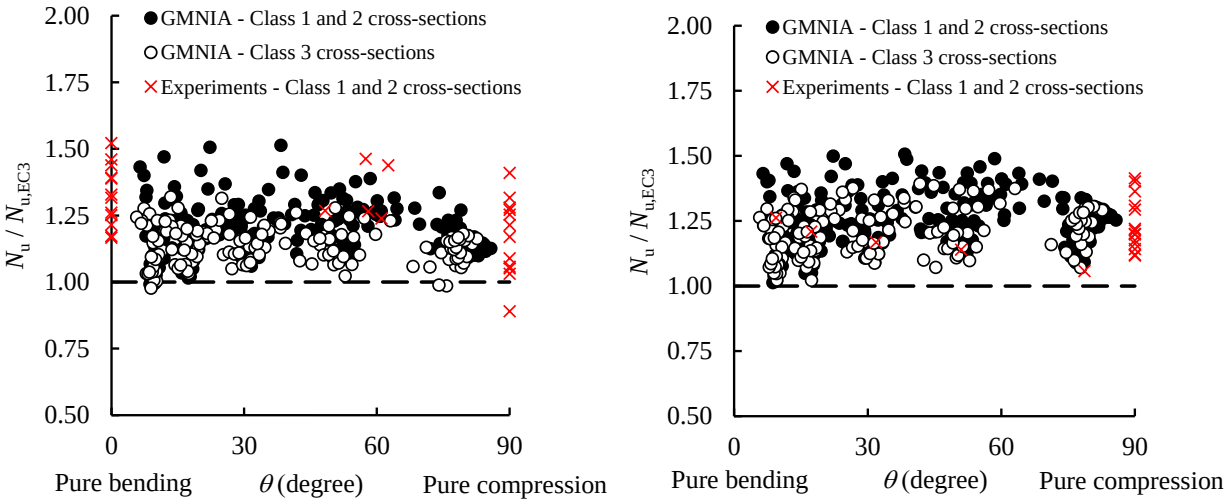

(a) Arc-welded beam-columns

(b) Laser-welded beam-columns

Figure 10: Assessment of EN 1993-1-4 design provisions for conventionally arc-welded and laser-welded beam-columns

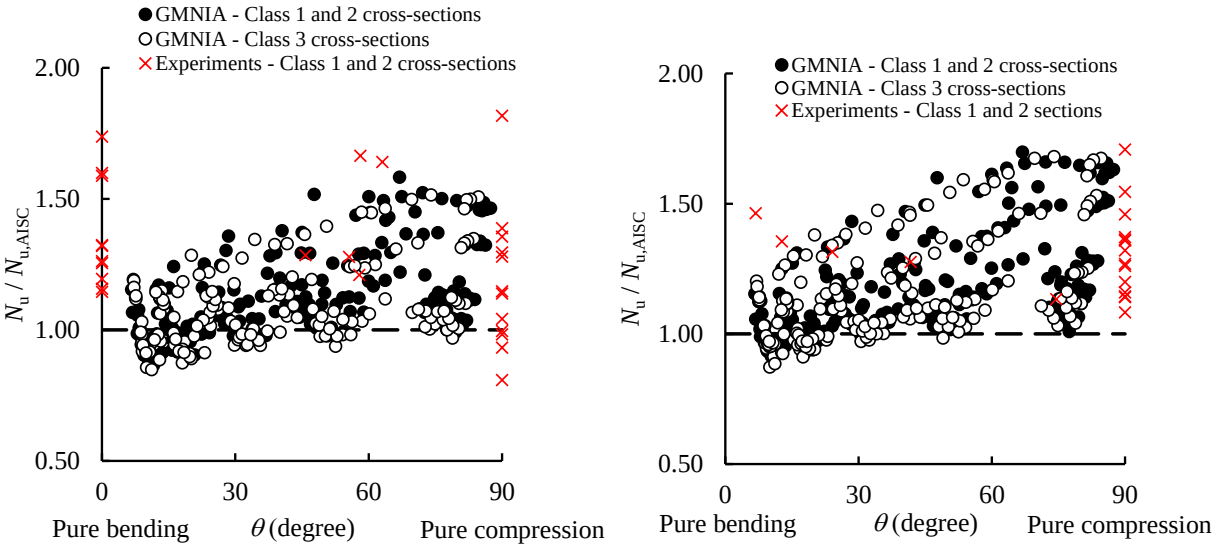

(a) Arc-welded beam-columns (b) Laser-welded beam-columns

Figure 11: Assessment of AISC Design Guide 27 [12] design provisions for conventionally arc-welded and laser-welded beam-columns

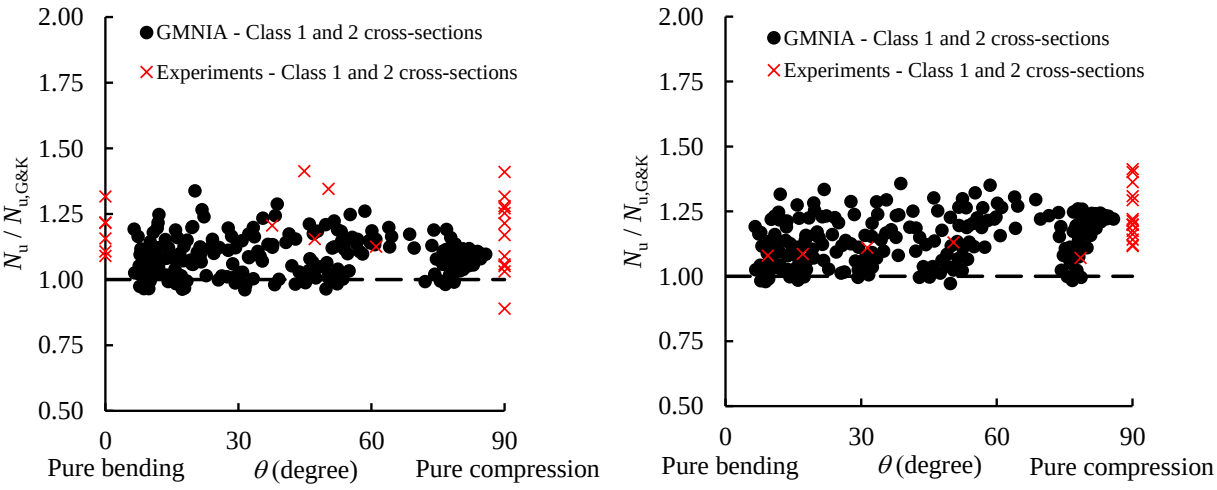

(a) Arc-welded beam-columns (b) Laser-welded beam-columns

Figure 12: Assessment of Greiner and Kettler [13] design provisions for conventionally arc-welded and laser-welded beam-columns

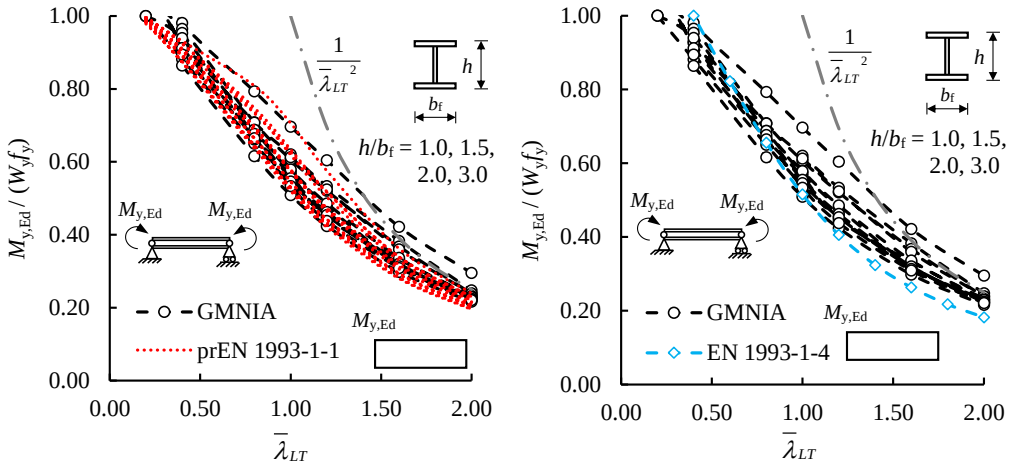

(a) prEN 1993-1-1 [41] (b) EN 1993-1-4 [2]

Figure 13: Accuracy assessment of the LTB assessment equations given in prEN 1993-1-1 [41] and EN 1993-1-4 [2] for arc-welded stainless steel beams under uniform bending

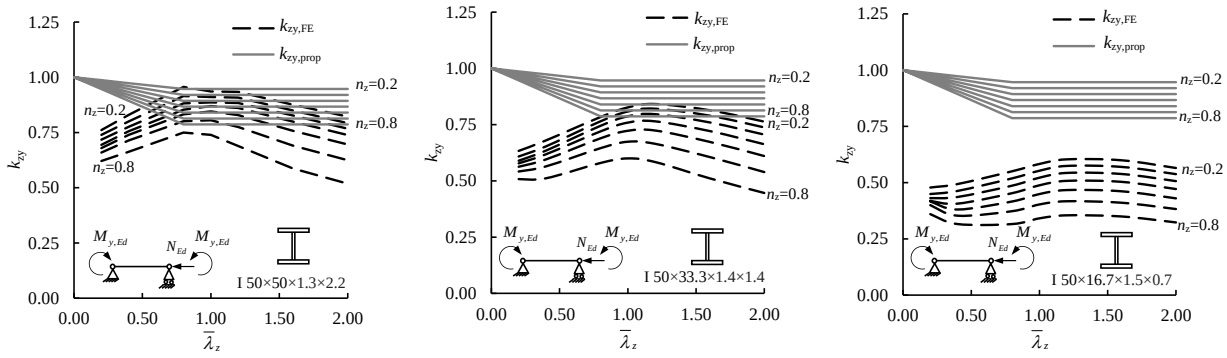

(a) I 50×50×1.3×2.2 (b) I 50×33.3×1.4×1.4 (c) I 50×16.7×1.5×0.7

Figure 14: Comparison of the proposed interaction factors $k_{zy,prop}$ against the numerically-determined interaction factors $k_{zy,FE}$ for austenitic stainless steel beam-columns with different cross-sections

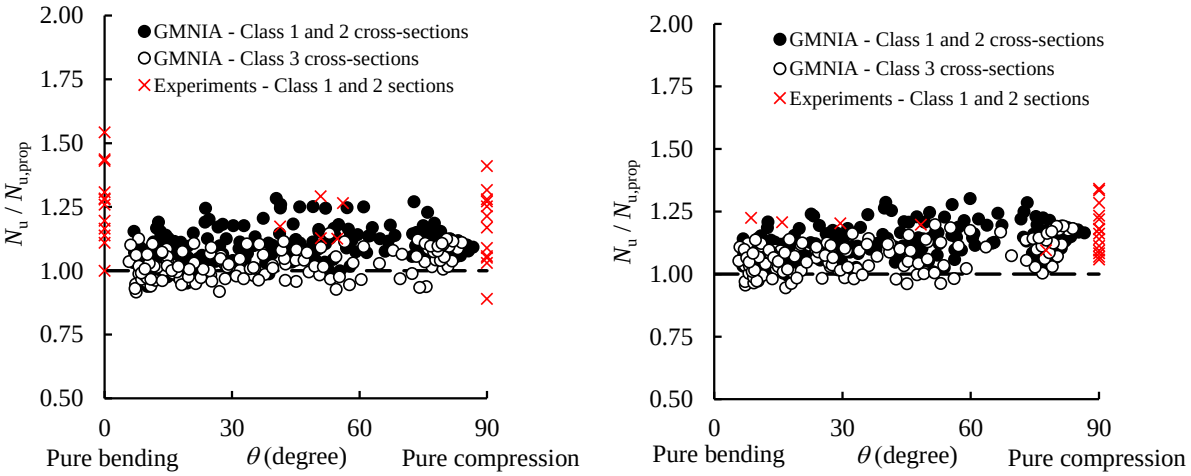

(a) Arc-welded beam-columns

(b) Laser-welded beam-columns

Figure 15: Accuracy of the proposals for the ultimate resistance predictions of arc-welded and laser-welded austenitic stainless steel beam-columns susceptible to flexural-torsional buckling

Tables captions

Table 1 : Summary of measured tensile and compressive material properties of I-50×50×4×4 section

Table 2 : Parameters used in the residual stress patterns for conventionally welded and laser-welded stainless steel I-sections

Table 3 : Measured geometric properties, imperfections and eccentricities of the specimens

Table 4 : Critical buckling lengths of the test specimens and non-dimensional slenderness for major axis flexural buckling $\overline{\lambda}_y$, minor axis flexural buckling $\overline{\lambda}_z$ and for lateral-torsional buckling (LTB) $\overline{\lambda}_{LT}$

Table 5 : Summary of experimental results for beam-column specimens

Table 6 : Comparisons of ultimate loads obtained from experiments and finite element simulations

Table 7 : Assessment of existing design methods for laterally-unrestrained stainless steel welded I-section beam-columns

Table 8 : Auxiliary coefficients used to determine the interaction factors for the design of laterally unrestrained I-section stainless steel beam-columns subjected to axial compression plus uniaxial major axis bending

Table 9 : Imperfection factors α and plateau lengths $\overline{\lambda}_0$ recommended for the determination of buckling resistances of conventionally arc-welded and laser-welded columns

Table 10 : Assessment of LTB equations provided in prEN 1993-1-1 [41] and EN 1993-1-4 [2] for arc-welded stainless steel beams under uniform bending

Table 11 : Auxiliary coefficients used to determine the interaction factors for the design of laterally unrestrained stainless steel I-section beam-columns subjected to axial compression plus uniaxial major axis bending

Table 12 : Assessment of proposed design method for laterally unrestrained welded austenitic stainless steel beam-columns susceptible to flexural-torsional buckling

Table 13 : Reliability analysis of the proposed design approach for arc-welded and laser-welded austenitic stainless steel beam-columns susceptible to flexural-torsional buckling

Table 14 : Interaction factors k_{yy} and k_{yz} for eq. (25). Instability governed by buckling about the y-y axis

Table 15 : Interaction factors k_{zy} and k_{zz} for eq. (26). Instability governed by buckling about the z-z axis

Table 1: Summary of measured tensile and compressive material properties of I-50×50×4×4 section

	E (MPa)	f_y (MPa)	$f_{1.0}$ (MPa)	f_u (MPa)	ϵ_u (%)	ϵ_f (%)	Compound R-O coefficients n	$m_{1.0}$	m_u
Tensile	190700	270	361	694	61	73	4.0	3.2	3.0
Compressive	206900	332	402	-	-	-	7.4	3.2	3.0

Table 2: Parameters used in the residual stress patterns for conventionally welded and laser-welded stainless steel I-sections

Welding type	$\sigma_{ft} = \sigma_{wt}$	$\sigma_{fc} = \sigma_{wc}$	a	b	c	d
Arc-welding [21]	$0.8f_y$	from equilibrium	$0.225b_f$	$0.050b_f$	$0.0250h_w$	$0.225h_w$
Laser-welding [5]	$0.5f_y$	from equilibrium	$0.100b_f$	$0.075b_f$	$0.0375h_w$	$0.100h_w$

Table 3: Measured geometric properties, imperfections and eccentricities of the specimens

Cross-section	Specimen ID	h (mm)	b_f (mm)	t_w (mm)	t_f (mm)	L (mm)	ω_g (mm)	e_n (mm)	e_m (mm)
I-50×50×4×4	50 LTB 2	50.44	50.53	4.00	4.01	1012.2	0.30	5	5.81
I-50×50×4×4	50 LTB 4	50.32	50.59	3.94	4.04	1014.0	0.06	20	21.67
I-50×50×4×4	50 LTB 5	50.47	50.55	3.99	3.99	1013.0	0.04	40	42.40
I-50×50×4×4	50 LTB 6	50.35	50.57	4.02	4.01	1012.5	0.30	80	82.88
I-50×50×4×4	50 LTB 7	50.30	50.62	4.00	4.01	1012.6	0.23	150	151.31

Table 4: Critical buckling lengths of the test specimens and non-dimensional slenderness for major axis flexural buckling $\overline{\lambda}_y$, minor axis flexural buckling $\overline{\lambda}_z$ and for lateral-torsional buckling (LTB) $\overline{\lambda}_{LT}$

Cross-section	Specimen ID	L (mm)	$L_{cr,y}$ (mm)	$L_{cr,z}$ (mm)	$\overline{\lambda}_y$	$\overline{\lambda}_z$	$\overline{\lambda}_{LT}$
I-50×50×4×4	50 LTB 2	1012.2	1162.2	506.1	0.73	0.53	0.43
I-50×50×4×4	50 LTB 4	1014.0	1164.0	507.0	0.73	0.53	0.43
I-50×50×4×4	50 LTB 5	1013.0	1163.0	506.5	0.73	0.53	0.44
I-50×50×4×4	50 LTB 6	1012.5	1162.5	506.2	0.73	0.53	0.43
I-50×50×4×4	50 LTB 7	1012.6	1162.6	506.3	0.73	0.53	0.43

Table 5: Summary of experimental results for beam-column specimens

Cross-section	Specimen ID	e_n (mm)	e_m (mm)	(ω_g+e_m) (mm)	$N_{ult,test}$ (kN)	$M_{y,ult,test}$ (kNm)	$u_{ult,test}$ (mm)
I-50×50×4×4	50 LTB 2	5	5.81	6.11	104.30	0.61	9.87
I-50×50×4×4	50 LTB 4	20	21.67	21.73	70.91	1.54	14.59
I-50×50×4×4	50 LTB 5	40	42.40	42.44	49.21	2.09	19.55
I-50×50×4×4	50 LTB 6	80	82.88	83.18	31.08	2.58	26.42
I-50×50×4×4	50 LTB 7	150	151.31	151.54	19.09	2.89	32.89

Table 6: Comparisons of ultimate loads obtained from experiments and finite element simulations

Cross-section	Specimen ID	e_m (mm)	$N_{ult,test}$ (kN)	$N_{ult,FE}$ (kN)	$\frac{N_{ult,test}}{N_{ult,FE}}$	$u_{ult,test}$ (mm)	$u_{ult,FE}$ (mm)	$\frac{u_{ult,test}}{u_{ult,FE}}$
I-50×50×4×4	50 LTB 2	5.81	104.30	109.06	0.96	9.87	8.56	1.15
I-50×50×4×4	50 LTB 4	21.67	70.91	72.66	0.98	14.59	16.55	0.88
I-50×50×4×4	50 LTB 5	42.40	49.21	49.50	0.99	19.55	17.71	1.10
I-50×50×4×4	50 LTB 6	82.88	31.08	31.01	1.00	26.42	23.94	1.10
I-50×50×4×4	50 LTB 7	151.31	19.09	18.85	1.01	32.89	28.77	1.14
				Average	0.99			1.08
				COV	0.020			0.104

Table 7: Assessment of existing design methods for laterally-unrestrained stainless steel welded I-section beam-columns

Design method	Welding type	Section class	N	ϵ_{av}	ϵ_{cov}	ϵ_{max}	ϵ_{min}
EN 1993-1-4 [2]	Arc-welded	Class 1 & 2	239	1.21	0.086	1.52	0.89
		Class 3	158	1.14	0.065	1.38	0.98
	Laser-welded	Class 1 & 2	243	1.25	0.081	1.51	1.01
		Class 3	166	1.21	0.077	1.40	1.02
AISC Design Guide 27 [12]	Arc-welded	Class 1 & 2	239	1.16	0.174	2.16	0.81
		Class 3	158	1.09	0.142	1.51	0.85
	Laser-welded	Class 1 & 2	243	1.19	0.166	1.71	0.91
		Class 3	166	1.16	0.171	1.68	0.87
Greiner and Kettler [13]	Arc-welded	Class 1 & 2	239	1.10	0.078	1.41	0.89
		Class 3	-	-	-	-	-
	Laser-welded	Class 1 & 2	243	1.11	0.104	1.36	0.90
		Class 3	-	-	-	-	-

Table 8: Auxiliary coefficients used to determine the interaction factors for the design of laterally unrestrained I-section stainless steel beam-columns subjected to axial compression plus uniaxial major axis bending

Buckling axis	Auxiliary coefficients	
Buckling about y-y axis ($k_{yy,prop}$)	$D_{1,y}$	2.50
	$D_{2,y}$	0.35
	$D_{3,y}$	1.00

Table 9: Imperfection factors α and plateau lengths $\overline{\lambda}_0$ recommended for the determination of buckling resistances of conventionally arc-welded and laser-welded columns

Axis of buckling	Welding type	α	$\overline{\lambda}_0$
Major axis (y-y)	Arc-welded	0.49	0.20
	Laser-welded	0.49	0.20
Minor axis (z-z)	Arc-welded	0.76	0.20
	Laser-welded	0.60	0.20

Table 10: Assessment of LTB equations provided in prEN 1993-1-1 [41] and EN 1993-1-4 [2] for arc-welded stainless steel beams under uniform bending

Design method	N	S_{av}	S_{cov}	S_{max}	S_{min}
prEN 1993-1-1 [41]	70	1.03	0.043	1.13	0.95
EN 1993-1-4 [2]	70	1.13	0.130	1.49	0.86

Table 11: Auxiliary coefficients used to determine the interaction factors for the design of laterally unrestrained stainless steel I-section beam-columns subjected to axial compression plus uniaxial major axis bending

Buckling axis	Auxiliary coefficients	
Buckling about z-z axis ($k_{zy,prop}$)	$D_{1,LT}$	0.20
	$D_{2,LT}$	0.40
	$D_{3,LT}$	0.80

Table 12: Assessment of proposed design method for laterally unrestrained welded austenitic stainless steel beam-columns susceptible to flexural-torsional buckling

Design method	Welding type	Section class	N	ϵ_{av}	ϵ_{cov}	ϵ_{max}	ϵ_{min}
Proposal	Arc-Welded	Class 1 & 2	239	1.10	0.070	1.41	0.89
		Class 3	158	1.03	0.051	1.15	0.92
	Laser-Welded	Class 1 & 2	243	1.12	0.063	1.34	0.99
		Class 3	166	1.07	0.056	1.20	0.95

Table 13: Reliability analysis of the proposed design approach for arc-welded and laser-welded austenitic stainless steel beam-columns susceptible to flexural-torsional buckling

Welding type	Data	N	b	$k_{d,n}$	V_δ	γ_{M1}
Arc-welded	Experiments & FE	397	1.07	3.44	0.080	1.12
	Experiments only	29	1.21	3.46	0.119	1.09
Laser-welded	Experiments & FE	409	1.10	3.44	0.063	1.06
	Experiments only	19	1.18	3.73	0.071	0.99

Table 14: Interaction factors k_{yy} and k_{yz} for eq. (25). Instability governed by buckling about the y-y axis

	Type of section	Interaction factor (k_{yy}, k_{yz})			Reference
		Austenitic	Duplex	Ferritic	
k_{yy}	I-sections	For $\overline{\lambda}_y < 1.0$: $k^*_{yy} = C_{my}[1+ 2.50(\overline{\lambda}_y - 0.35)n_y]$	–	–	[7]
		For $\overline{\lambda}_y \geq 1.0$: $k^*_{yy} = C_{my}(1+ 1.625n_y)$	–	–	
	SHS & RHS	For $\overline{\lambda}_y < 1.3$: $k_{yy} = C_{my}[1+ 2.00(\overline{\lambda}_y - 0.30)n_y]$	For $\overline{\lambda}_y < 1.4$: $k_{yy} = C_{my}[1+ 1.50(\overline{\lambda}_y - 0.40)n_y]$	For $\overline{\lambda}_y < 1.6$: $k_{yy} = C_{my}[1+ 1.30(\overline{\lambda}_y - 0.45)n_y]$	[38]
		For $\overline{\lambda}_y \geq 1.3$: $k_{yy} = C_{my}(1+ 2n_y)$	For $\overline{\lambda}_y \geq 1.4$: $k_{yy} = C_{my}(1+ 1.5n_y)$	For $\overline{\lambda}_y \geq 1.6$: $k_{yy} = C_{my}(1+ 1.495n_y)$	
	CHS	For $\overline{\lambda}_y < 1.3$: $k^*_{yy} = C_{my}[1+ 2.50(\overline{\lambda}_y - 0.30)n_y]$	For $\overline{\lambda}_y < 1.3$: $k^*_{yy} = C_{my}[1+ 2.00(\overline{\lambda}_y - 0.38)n_y]$	For $\overline{\lambda}_y < 1.3$: $k^*_{yy} = C_{my}[1+ 1.90(\overline{\lambda}_y - 0.35)n_y]$	[45]
		For $\overline{\lambda}_y \geq 1.3$: $k^*_{yy} = C_{my}(1+ 2.5n_y)$	For $\overline{\lambda}_y \geq 1.3$: $k^*_{yy} = C_{my}(1+ 1.84n_y)$	For $\overline{\lambda}_y \geq 1.3$: $k^*_{yy} = C_{my}(1+ 1.805n_y)$	
k_{yz}	I-sections SHS RHS CHS	$k_{yz} = k_{zz}$ (for k_{zz} see Table 15)			

*Note that this formula has only been verified for members under uniform bending; for other shapes of bending moment diagrams, the formulae has not been verified but use of the prEN 1993-1-1 [41] C_m factors are recommended at present.

Table 15: Interaction factors k_{zy} and k_{zz} for eq. (26). Instability governed by buckling about the z-z axis

	Type of section	Interaction factor (k_{zy}, k_{zz})			Reference
		Austenitic	Duplex	Ferritic	
k_{zy}	I-sections	For $\overline{\lambda}_z < 0.8$: $k^*_{zy} = 1 - \frac{0.2\overline{\lambda}_z n_z}{C_{mLT}-0.4}$	–	–	This study
		For $\overline{\lambda}_z \geq 0.8$: $k^*_{zy} = 1 - \frac{0.16 n_z}{C_{mLT}-0.4}$	–	–	
	SHS RHS CHS	$k_{zy} = k_{yy}$ (for k_{yy} see Table 14)			
k_{zz}	I-sections	For $\overline{\lambda}_z < 1.2$: $k^*_{zz} = C_{mz}[1+ 2.80(\overline{\lambda}_z - 0.50)n_z]$	For $\overline{\lambda}_z < 1.2$: $k^*_{zz} = C_{mz}[1+ 2.80(\overline{\lambda}_z - 0.50)n_z]$	For $\overline{\lambda}_z < 1.2$: $k^*_{zz} = C_{mz}[1+ 2.80(\overline{\lambda}_z - 0.50)n_z]$	[7]
		For $\overline{\lambda}_z \geq 1.2$: $k^*_{zz} = C_{mz}(1+ 1.96 n_z)$	For $\overline{\lambda}_z \geq 1.2$: $k^*_{zz} = C_{mz}(1+ 1.96 n_z)$	For $\overline{\lambda}_z \geq 1.2$: $k^*_{zz} = C_{mz}(1+ 1.96 n_z)$	
	SHS & RHS	For $\overline{\lambda}_z < 1.3$: $k_{zz} = C_{mz}[1+ 2.00(\overline{\lambda}_z - 0.30)n_z]$	For $\overline{\lambda}_z < 1.4$: $k_{zz} = C_{mz}[1+ 1.50(\overline{\lambda}_z - 0.40)n_z]$	For $\overline{\lambda}_z < 1.6$: $k_{zz} = C_{mz}[1+ 1.30(\overline{\lambda}_z - 0.45)n_z]$	[38]
		For $\overline{\lambda}_z \geq 1.3$: $k_{zz} = C_{mz}(1+ 2 n_z)$	For $\overline{\lambda}_z \geq 1.4$: $k_{zz} = C_{mz}(1+ 1.5 n_z)$	For $\overline{\lambda}_z \geq 1.6$: $k_{zz} = C_{mz}(1+ 1.495 n_z)$	
	CHS	For $\overline{\lambda}_z < 1.3$: $k^*_{zz} = C_{mz}[1+ 2.50(\overline{\lambda}_z - 0.30)n_z]$	For $\overline{\lambda}_z < 1.3$: $k^*_{zz} = C_{mz}[1+ 2.00(\overline{\lambda}_z - 0.38)n_z]$	For $\overline{\lambda}_z < 1.3$: $k^*_{zz} = C_{mz}[1+ 1.90(\overline{\lambda}_z - 0.35)n_z]$	[45]
		For $\overline{\lambda}_z \geq 1.3$: $k^*_{zz} = C_{mz}(1+ 2.5 n_z)$	For $\overline{\lambda}_z \geq 1.3$: $k^*_{zz} = C_{mz}(1+ 1.84 n_z)$	For $\overline{\lambda}_z \geq 1.3$: $k^*_{zz} = C_{mz}(1+ 1.805 n_z)$	

*Note that this formula has only been verified for members under uniform bending; for other shapes of bending moment diagrams, the formulae has not been verified but use of the prEN 1993-1-1 [41] C_m factors are recommended at present.